



Chemical, Elemental and Structural Analysis of Batteries

Application Compendium

Contents

Imaging techniques for 2D/3D morphology	Raman	<i>Ex situ</i> Raman Analysis of Lithium Ion Batteries	3
		<i>In situ</i> Raman Analysis of Lithium Ion Batteries	6
		Raman Analysis of Lithium-Ion Battery Components – Part I: Cathodes	10
		Raman Analysis of Lithium-Ion Battery Components – Part II: Anodes	14
		Raman Analysis of Lithium-Ion Battery Components – Part III: Electrolytes	19
Bulk analysis	SEM	Investigate batteries with a SEM for better performance	22
	microCT	Uncovering Internal Structure Defects in Lithium Ion Battery Foils	25
	XPS	Analysis of Electrode Materials for Lithium Ion Batteries	27
	Ion Chromatography	Determination of Electrolyte Solution from Lithium Ion Battery	30
		Determination of Dissolved Manganese in Lithium/Manganese Oxide Battery Electrolyte	35
	ICP-OES	Simultaneous Determination of Impurities and Major Elements in Lithium-ion Battery Cathodes	39
	GC-MS	Orbitrap GC-MS Technology Provides New Insight into Lithium Ion Battery Degradation	44

The global lithium-ion battery market is expected to reach 93.1 billion USD by 2025. This is largely driven by increased usage in electric vehicles, grid storage, and portable consumer electronics where the higher energy density of the lithium-ion battery offers a clear advantage.

Increases in battery performance requires the development of new battery components as well as understanding and addressing the mechanisms that result in performance degradation with repeated charging and discharging cycles. Evaluation of batteries and battery components requires a variety of analytical methods that study materials and component surfaces at various scales.

As the world leader in advancing science, Thermo Fisher Scientific provides the widest range of analytical instrumentation for battery analysis and product formulation, including X-ray photoelectron spectroscopy (XPS/ESCA), electron microscopy (SEM, TEM and FIB-SEM), vibrational spectroscopy (FTIR, Raman and NIR), mass spectrometry (GC-MS, HPLC, LC-MS, HREMS-MS, ICP-MS), microCT, nuclear magnetic resonance (NMR), X-ray diffraction, X-ray fluorescence, rheometry, viscometry, extrusion and torque rheometry.

Imaging techniques such as Raman, microCT, and electron microscopy cover the full length scale from the cell level with Raman and microCT down to the atomic scale with TEM. Raman imaging can be used to observe the distribution of components and to monitor how these components change during the charging/discharging cycles. MicroCT and electron microscopy

are mainly used to study the 2D and 3D morphology of battery components at different stages in the life cycle. 3D imaging provides complete geometric evolution of the cathode micro-structure upon cycling. Geometric parameters such as volume fraction, surface area, particle size distribution and tortuosity are typically assessed using a combination of microCT and FIB-SEM techniques.

Spectroscopy, NMR, X-ray diffraction and mass spectrometry are key to studying the evolution of structural and chemical changes and the defect formation in battery electrodes. These techniques permit the analysis of electrode materials as they change during the redox reactions; and give information on both crystalline and amorphous phases. Local differences in Raman spectral changes can create a state-of-charge (SOC) distribution map showing the composite electrode. The composition of the solid electrolyte interface (SEI) is commonly studied with ex situ XPS and in situ FTIR and Raman spectroscopy to monitor the SEI formation.

Rheology and viscometry systems measure the dispersiveness and coating capability of battery materials in an electrode slurry. Torque rheometers deliver information about melting behavior, influence of additives on processability and temperature or shear stability; all critical parameters for the production of polymer separators.

This compendium of application notes provides in-depth reports on analyses aimed at improving the performance of lithium-ion batteries.

Find out more about Thermo Fisher Scientific capabilities for batteries at thermofisher.com/energy

Ex situ Raman Analysis of Lithium Ion Batteries

Author

Dick Wieboldt, Ph.D., Thermo Fisher Scientific, Madison, WI, USA

Key Words

Anodes, *Ex Situ* Analysis, Lithium Ion Battery, Raman Microscopy, Raman Imaging

Abstract

The needs of the Li-ion battery customers can be segmented into *in situ* and *ex situ* modes of analysis. *Ex situ* analysis lets researchers study battery components removed from the operating battery cell.

Introduction

Analysis of battery materials with Raman spectroscopy has been around for quite some time. During the 1960s, researchers used Raman to elucidate many of the fundamental spectral features of the minerals and inorganic materials widely used in battery research today.^{1,2} Raman is a good fit for these materials because many of the characteristic vibrational and rotational modes occur in the low-wavenumber region of the spectrum typically accessible only by far-infrared measurements. In that day and age, both Raman and far-infrared measurements were time consuming and difficult experiments.

Analysis Techniques: *In situ* Versus *Ex situ*

The term *in situ* is used to describe experiments where the battery components are studied in an assembled cell under operating conditions. Think of *in situ* as a window on the case of a battery which lets you see the chemistry of what goes on when you charge and discharge a battery.

While *in situ* cells provide valuable information, their use is generally targeted at research and development of new materials for Li-ion batteries. Once a formulation is designed, a candidate battery is scaled up through pilot production to actual product samples. At this stage of development, researchers



are most interested in characterizing failure modes and a better understanding of performance differences. For example, what makes one production run work better than another, and why did one battery fail yet its siblings from the same batch worked fine.

To answer these questions, researchers carefully disassemble a battery cell so the individual components can be examined. This type of analysis is termed *ex situ* because the battery components are removed from the operating battery cell. The goal is to prepare the samples for analysis in as close to a native state as possible.

Battery disassembly for *ex situ* analysis is carried out in an inert environment such as an argon filled glove box to protect the battery components from moisture and oxidation. For example, the anode, separator, cathode sandwich must be carefully separated and rinsed to remove excess electrolyte.

Once the samples are prepared, they must be kept in an inert environment to protect against changes during analysis. When space is available, instruments are installed inside the glove box so the samples can be analyzed. In most cases, the sample must be removed from the glove box and transferred to an external instrument for analysis. This is where an ex situ transfer cell becomes a key component of the workflow. It preserves the inert environment around the sample so it can be studied.

From Single Point Measurements to Raman Imaging

The majority of published research on Li-ion battery Raman work is based on single point measurements acquired over time during charge/discharge cycles. Single point measurements can be misleading because there is no way of knowing if the sampled point is representative of the entire electrode. It is important to make multiple measurements to be sure. Because the Raman signals are weak, it takes many minutes to generate enough signal-to-noise ratio at each measurement point. A complete, multi-point experimental can be quite time consuming to complete.

Today, Raman imaging is a viable alternative which lets you quickly makes thousands of measurements over an area of the electrode rather than just single point measurements. Each pixel in a Raman image is a complete Raman spectrum. This technique provides confidence in understanding if changes are heterogeneous or hot spots.

The following experimental results demonstrate the flexibility of using Raman imaging for the ex situ analysis of Li-ion batteries and their components.

Characterization of Li-ion Anodes

After safety concerns, a leading area of interest in Li-ion battery research is understanding the cause of performance degradation over time. Research indicates the solid electrolyte interphase (SEI) layer formed on the surface of the electrode is key to performance. The SEI layer is formed by deposition of organic and inorganic compounds during the first several charge/discharge cycles.⁴ It stabilizes the electrode from further decomposition and promotes reversible capacity. Because of the complexity of the SEI layer, results from any and all analytical techniques contribute to an incremental understanding of its behavior.

As you might expect, it is a messy business to extract electrodes from a used battery so the SEI can be studied. It takes great care to prepare the sample so as to preserve its integrity for ex situ analysis. This is usually achieved by working in an argon filled glove box to prevent sample degradation due to atmospheric exposure. A transfer cell with window is used to seal the sample in the inert argon environment so it can be removed from the glove box for analysis using a Raman microscope.

Experimental

Anode samples from a disassembled Li-ion battery were cut and mounted in a Thermo Scientific™ transfer cell so that a cross-section of the anode could be imaged.

The transfer cell (Figure 1) maintains an inert environment surrounding the sample so it can be analyzed using instruments outside a glove box. The cell body accepts a variety of industry standard sample holders (stubs) developed for scanning electron microscope (SEM) analysis. A 90° stub was used to hold the cut edge of the anode facing the window. A cap containing a calcium fluoride (CaF₂) window seals the sample under an argon blanket. The cap is screwed on until the window height is just above the sample. This provides a minimum working distance between a microscope objective and the sample. A short working distance is an advantage because it allows the use of high magnification objectives having a large numerical aperture (N.A.).

Raman spectra were collected over a single 76 μm \times 160 μm area at spatial resolution of 1.0 μm per pixel using a Thermo Scientific™ DXR™xi Raman imaging microscope. Laser power at the sample was 2.0 mW at 532 nm with a 0.2 sec exposure time and 4 image scans. An Olympus™ 50 \times long working distance, 0.5 N.A. microscope objective was used to focus through the transfer cell window. Higher laser powers and/or longer exposure times were avoided because they can heat the sample causing changes which mask the native state of the electrode.



Figure 1: Transfer cell maintains sample in an inert environment for ex situ analysis of Li-ion battery materials

Results

A Raman image is a hyperspectral data set with each pixel in the image being a complete Raman spectrum. Using a variety of spectral processing techniques, this hyperspectral Raman data generates image contrast pertaining to specific chemical features. This capability is used to visualize minute differences within a sampled area.

A variety of chemical images can be created from each data set showing changes within the sampled area. For this experiment, image contrast is generated by multivariate curve resolution (MCR) analysis. MCR finds the major components within each image and a different color is assigned to each. This is analogous to the use of dyes in biological fluorescence imaging which tag different parts of a cell.

Alternatively, multiple regions of the sample can be imaged and the Raman spectral data within each region can be averaged to produce a single spectrum. In this mode, the Raman imaging data set is used as a means of homogenizing any differences in the electrode area. This average spectrum represents a single point measurement yet each point represents a 30 μm square compared with the typical 1 μm sample area from a standard Raman microscope.

Figure 2 is a micrograph of the anode cross section. The copper current collector is in the center with anode material coated on both surfaces. Superimposed is the Raman image created from the spectral differences shown by the inset Raman spectra. The Raman image clearly shows that the coating on one side of the copper current collector is dominated by carbon black (red) whereas the other side has a much greater density of the active graphite phase (blue).

This example demonstrated the advantage of Raman imaging over traditional single point measurements. The major differences in the two coatings could easily have been missed by single point measurements depending on where the points were measured.

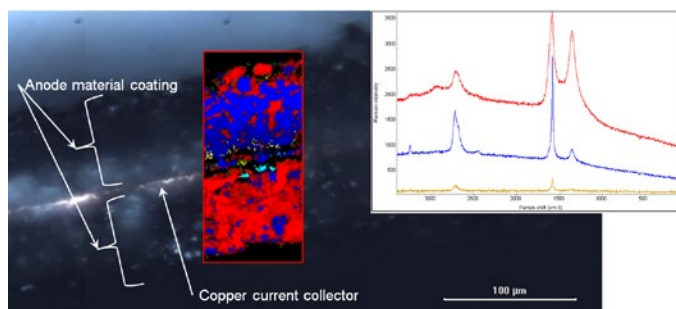


Figure 2: Cross section view of a Li-ion battery anode. Raman image indicates a difference in the anode coating on each side. Inset Raman spectra are color coded to the areas in the Raman image.

Conclusion

The high sensitivity of Raman imaging is a benefit for Li-ion battery analysis. Ex situ Raman imaging measurements give results with a higher degree of confidence compared to single points.

References

1. P. Tarte, J. Inorg. Nucl. Chem. 29(4) 915–923 (1967).
2. W.B. White, B.A. De Angelis, Spectrochimica Acta Part A 23(4) 985–995 (1967).
3. R. Baddour-Hadjean, J.P. Pereira-Ramos, Chemical Reviews 110(3) 1278–1319 (2010).
4. A. Chagnes and J. Swiatowska, Electrolyte and Solid-Electrolyte Interphase Layer in Lithium-Ion Batteries, Lithium Ion Batteries – New Developments, Dr. Ilias Belharouak (Ed.), ISBN: 978-953-51-0077-5, InTech, (2012). Available from: <http://www.intechopen.com/books/lithium-ion-batteries-newdevelopments/electrolyte-and-solid-electrolyte-interphase-layer-in-lithium-ion-batteries>.

In situ Raman Analysis of Lithium Ion Batteries

Author

Dick Wieboldt, Ph.D., Thermo Fisher Scientific, Madison, WI, USA
Ines Ruff, Ph.D., Thermo Fisher Scientific, Dreieich, Germany
Matthias Hahn, Ph.D., El-Cell GmbH, Homburg, Germany

Key Words

Electrodes, *In Situ* Analysis, Lithium Ion Battery, Raman Microscopy, Raman Imaging

Abstract

The needs of the Li-ion battery customers can be segmented into *in situ* and *ex situ* modes of analysis. *In situ* analysis allows researchers to follow changes in a battery cell during its charge and discharge cycles. Recent improvements in Raman sensitivity enable these changes to be imaged on a dynamic time scale.

Introduction

The use of Raman spectroscopy for analysis of battery materials has been around for years. During the 1960s, researchers used Raman to elucidate many of the fundamental spectral features of the minerals and inorganic materials widely used in battery research today.^{1,2} Raman is a good fit for these materials because many of the characteristic vibrational and rotational modes occur in the low-wavenumber region of the spectrum typically accessible only by far-infrared measurements. In that day and age, both Raman and far-infrared measurements were time consuming and difficult experiments.

Advances in instrumentation have greatly increased the ease-of-use of Raman making it a much more approachable technique. New areas of application ensued such as the exploding interest in rechargeable lithium ion batteries. Many researchers are involved and have published careful studies of materials specifically related to Li-ion batteries as well as next generation batteries. A review article by Baddour-Hadjean published in 2010 is an excellent resource for those wishing to get up-to-speed in this field.³ The focus of this application note is on the *in situ* application of Raman spectroscopy as it pertains to battery research.



Analysis Techniques: *In situ* Versus *Ex situ*

The term *in situ* is used to describe experiments where the battery components are studied in an assembled cell under operating conditions. Think of *in situ* as a window on the case of a battery which lets you see the chemistry of what goes on when you charge and discharge a battery. There are very few commercially available cell designs compatible with spectroscopic measurements. Researchers have resorted to building their own cells to meet the needs of their experimental apparatus. Examples of such designs have been published along with experimental results.⁴⁻¹⁰

In situ cells analysis is generally targeted at research and development of new materials for Li-ion batteries. Once a formulation is designed, a candidate battery is scaled up through pilot production to actual product samples. At this stage of development, researchers are most interested in characterizing failure modes and a better understanding of performance differences. For example, what makes one production run work better than another, and why did one battery fail yet its siblings from the same batch worked fine.

To answer these questions, researchers carefully disassemble a battery cell so the individual components can be examined. This type of analysis is termed *ex situ* because the battery components are removed from the operating battery cell. The goal is to prepare the samples for analysis in as close to a native state as possible. Please see the companion application note for details on *ex situ* analysis.

From Single Point Measurements to Raman Imaging

The majority of published research on Li-ion battery *in situ* Raman work is based on single point measurements acquired over time during charge/discharge cycles. An example is the excellent work done by Kostecki's group at Lawrence Berkeley National Lab.¹¹

Single point measurements can be misleading because there is no way of knowing if the sampled point is representative of the entire electrode. It is important to make multiple measurements to be sure. Because the Raman signals are weak, it takes many minutes to generate enough signal-to-noise ratio at each measurement point. A complete, multi-point experiment can be quite time consuming to complete.

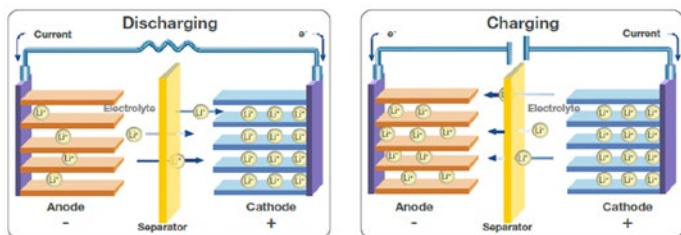


Figure 1: Movement of Li^+ ions balance electrons during the charge and discharge cycles of a Li-ion battery

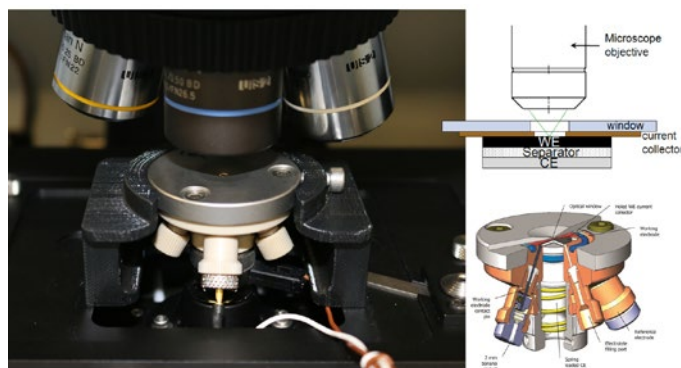


Figure 2: Experimental setup for the in situ example showing the electrochemical cell mounted on the stage of a Raman imaging microscope

Today, Raman imaging is a viable alternative which lets you quickly make thousands of measurements over an area of the electrode rather than just single point measurements. Each pixel in a Raman image is a complete Raman spectrum. This technique provides confidence in understanding if changes are heterogeneous or hot spots.

The following experimental results demonstrate the flexibility of using Raman spectroscopy for *in situ* analysis of Li-ion batteries and their components.

Lithiation of Graphite

Graphite is widely used as an anode material for rechargeable Li-ion batteries.

During the Li-ion battery charging cycle, positively charged Li^+ ions move from cathode through the electrolyte, across a separator into the anode to balance the flow of electrons in the external circuit (Figure 1). This process of Li^+ ions entering the graphitic structure of the anode is called intercalation. Intercalation causes changes in the anode structure – primarily a swelling of the graphite structure.

Experimental

The experimental setup for this example consists of a Thermo Scientific™ DXR™xi Raman imaging microscope and an EL-CELL® ECC-Opto-Std optical electrochemical cell. This cell enables the investigation of batteries in a so-called sandwich configuration where the working electrode (WE) material is placed under a sapphire (Al_2O_3) window. Electrode material (graphite powder in this example) is spread onto a copper grid serving as the current collector. This WE is sandwiched from below, with a glass fiber separator soaked with the electrolyte solution and lithium metal as the counter electrode (CE).

The Raman beam from the microscope objective impinges onto the backside of the WE material through the sapphire window (Figure 2). The advantage of investigating the backside of the electrode is that the pathway for the Raman beam is minimized, allowing the use of high magnification objectives, optimizing spectra quality. The drawback is the gradient of lithiation concentration along the depth of the electrode. Accordingly, the electrode must be charged very slowly in order to minimize this unwanted gradient.

The graphite electrode was cycled at a constant rate of approximately 0.06 C. The C-rate is measure of how rapidly a battery is charged/discharged. This rate of 0.06 C corresponds to 33 hours for a full charge/discharge cycle between 1.5 and 0.005 V against Li/Li^+ . Raman imaging was carried out during the initial 480 minutes of the charging (lithiation) process only.

Raman spectra were collected over a $30\text{ }\mu\text{m} \times 30\text{ }\mu\text{m}$ area at $1\text{ }\mu\text{m}$ pixel spacing using 2 mW of 532 nm laser excitation, a 0.01 sec exposure time for each pixel, and 50 scans per image. Higher laser powers and/or longer exposure times resulted in burning of the graphite and boiling of the electrolyte.

Results

A Raman image is a hyperspectral data set with each pixel in the image being a complete Raman spectrum. Using a variety of spectral processing techniques, this hyperspectral Raman data generates image contrast pertaining to specific chemical features. It is this capability that visualizes minute differences within a sampled area. By collecting a sequence of Raman images, we now have the ability to monitor changes in both space and time. As mentioned earlier, a variety of chemical images can be created from each data set showing changes within the sampled area. Alternatively, the Raman spectral data within each data set can be averaged to produce a single spectrum for each time slice. In this mode, the Raman imaging data set is used as a means of homogenizing any differences in the electrode area. This average spectrum represents a single point measurement yet each point represents a $30\ \mu\text{m}$ square compared with the typical $1\ \mu\text{m}$ sample area from a standard Raman microscope.

$1\ \mu\text{m}$ sample area from a standard Raman microscope.

In Figure 3, the 3D view (bottom left) shows changes in the Raman spectrum as a function of time over 8.3 hours (1–500 min). During this time, the battery cell is in the charging (lithiation) process only. This portion of the electrochemical cycle is shown in the lower right of Figure 3.

The spectrum of graphite exhibits a prominent peak at $1580\ \text{cm}^{-1}$ attributed to the E_{2g} mode (G band). At potentials between 0.42 and 0.31 V (specific charge 33 and 45 mAh/g), the band gradually disappears along with the simultaneous emergence of a peak centered at $1590\ \text{cm}^{-1}$. This peak shift is attributed to the Li^+ ions intercalated into the graphite structure. This is more easily seen in the center, 2D Raman image. The inset shows Raman spectra before and after the change.

Towards the end of the charge cycle at 8.3 hours (496 min), where the voltage is less than 0.15 V (specific charge greater than 146 mAh/g), a strong Raman band centered at $154\ \text{cm}^{-1}$ begins to appear. This Raman band has not been previously reported so its assignment is not conclusive. Strong Raman bands in this region have been attributed to TiO_2 , Sb, and metal chlorides.

The type of views shown in Figure 3 are “spectrum-centric” because they show changes in the Raman spectra captured at different times during a time based analysis. Figure 4 shows another way of exploring the same Raman imaging data set from an alternative “image-centric” point-of-view. Here, we are not as interested in the Raman spectrum itself but rather its use as a tool to enhance differences within the image (image contrast).

In Figure 4, Raman images are presented in which the image contrast is generated by multivariate curve resolution (MCR) analysis. In this case, MCR finds the differences not only within each image but also across the entire time sequence. A different color is assigned to each resolved component. This is analogous to the use of dyes in biological fluorescence imaging which tag different parts of a cell. Each image is from the same $30\ \mu\text{m}$ square portion of the anode. The blue MCR component is indicative of the $1580\ \text{cm}^{-1}$ band; green the $1590\ \text{cm}^{-1}$ band; yellow the $154\ \text{cm}^{-1}$ band; red represents carbon black, a conductivity enhancer.

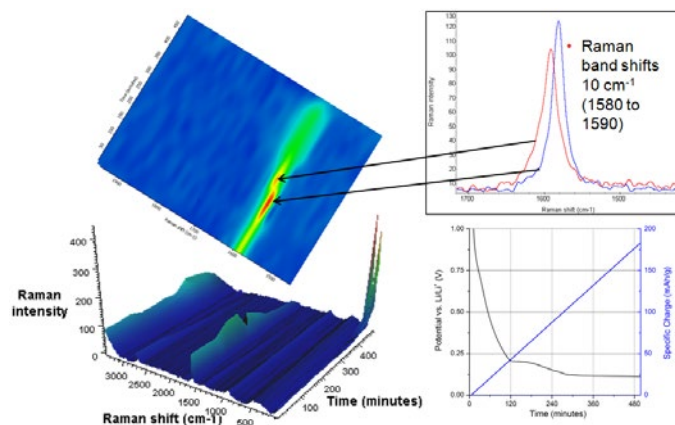


Figure 3: Different views rendered from the time lapse hyperspectral Raman data provide a wealth of experimental information

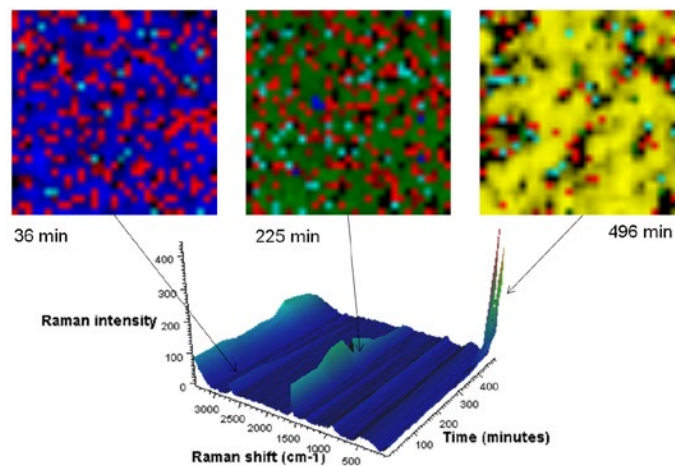


Figure 4: Raman images from different time slices in the graphite lithiation experiment

It can be challenging to visualize the information content with such a massive wealth of data. Figure 4 shows just three frames to demonstrate this type of analysis. The changes are easier to grasp using a time lapse viewer of the complete time sequence:

- 3D time lapse: <http://youtu.be/lc0MFAB5U4M>
- Time lapse: <http://youtu.be/geq6mbYVARE>

Conclusion

The high sensitivity of Raman imaging is a benefit for Li-ion battery analysis. *In situ* Raman imaging techniques show the spatial distribution of phase changes in electrodes over time. This is a capability that was not possible with single point measurements using traditional Raman microscopy.

References

1. P. Tarte, J. Inorg. Nucl. Chem. 29(4) 915–923 (1967).
2. W.B. White, B.A. De Angelis, Spectrochimica Acta Part A 23(4) 985–995 (1967).
3. R. Baddour-Hadjean, J.P. Pereira-Ramos, Chemical Reviews 110(3) 1278–1319 (2010).
4. T. Gross, C. Hess, J Power Sources 256, 220–225 (2014).
5. P. Novák, D. Goers, L. Hardwick, M. Holzapfel, W. Scheifele, J. Ufheil, A. Wursig, J Power Sources 146, 15–20 (2005).
6. C.M. Burba, R. Frech, Applied Spectroscopy 60(5), 490–493 (2006).
7. E. Markevich, V. Baranchugov, G. Salitra, D. Aurbach, M. Schmidt, J Electrochem Soc 155(2), A132–A137 (2008).
8. Y. Luo, W.B. Cai, X.K. Xing, D.A. Scherson, Electrochem. Solid-State Lett. 7(1), E1–E5 (2004).
9. T. Gross, L. Giebeler, C. Hess, Rev. Sci. Instrum. 84(7), 073109-1–073109-6 (2013).
10. K. Hongyou, T. Hattori, Y. Nagai, T. Tanaka, H. Nii, K. Shoda, Power Sources 243, 72–77 (2013).
11. J. Lei, F. McLarnon, R. Kostecki, J. Phys. Chem. B, 109(2), 952–957 (2005).

Raman analysis of lithium-ion battery components

Part I: Cathodes

Author

Robert Heintz, Ph.D., Thermo Fisher Scientific
Madison, WI, USA

Keywords

DXR 2 Microscope, cathodes, lithium-ion battery, Raman

Introduction

In recent years the increasing demand for powering portable electronic devices from laptops to smart phones has driven the need for improved battery performance but the emergence of electric and hybrid vehicles is creating additional interest in new battery technologies. The expanding use of portable energy storage introduces additional factors beyond just improving battery capacity. Cost, safety, and environmental impact are important considerations as the use of battery technology evolves. Lithium-ion batteries offer the highest energy density and output voltage among commercial rechargeable battery systems.¹ Even though lithium-ion batteries are now an established technology there is still considerable interest in improving the current technology and the development of new battery components.

Evaluation of batteries and battery components requires a variety of analytical methods not only for the development of new materials but also for gaining a greater understanding of the mechanisms involved in charge/discharge cycles. Bulk analysis of components is important but it is also important to understand surface interactions and interfaces. Electrochemical evaluation of cells includes conductivity measurements, electrochemical stability of components, cell capacity, ion mobility, discharge rates, and cycling behavior. Materials characterization of the various cell components can include many different analytical techniques (examples: XRD, SEM, TEM, TGA, DSC, EDS) but one technique that is rapidly growing in popularity for the analysis of materials is Raman spectroscopy. Raman spectroscopy has many advantages but the most important for battery applications are ones that involve subtle changes in



molecular structure or local chemical environments. The spectral results can usually be correlated with the electrochemical performance.

There have been significant improvements in commercial Raman instrumentation over the last several years. Important advances in both hardware and software have made modern Raman instruments much more user friendly and removed many of the obstacles that in the past made routine use of Raman spectroscopy arduous for users with limited expertise. Advances in instrumentation also include integration of light microscopes with Raman instrumentation which allows spectroscopic analysis of samples at the microscopic level. Modern Raman instruments, like the Thermo Scientific™ DXR™ 2 Raman microscope, are fully integrated, high performance research grade instruments that have incorporated extensive automation to simplify the collection of Raman spectra. For example, automated on-demand alignment and calibration present on the DXR 2 microscope, is designed to eliminate the need for manual realignment and calibration and results in an instrument that is easy to use and maintain at its highest level of performance. This ease of use means it is much quicker to get started and straightforward to get accurate results. This opens up the use of Raman spectroscopy for all types of users.

Raman has been used for the analysis of many different types of battery components. This includes analysis of cathode materials, anode materials, and electrolytes.^{2,3} Part one of this series will focus on some examples of how Raman spectroscopy has been utilized for the analysis of cathode materials. This article is in no way meant as a complete review of the literature. That is beyond the scope of this application note. Included here are some interesting examples from published papers that illustrate how Raman spectroscopy has been used for the analysis of cathode materials.

Developing new cathode materials for lithium ion batteries has been a very active area of research. LiCoO_2 is the classical cathode material for lithium ion batteries but there are issues with the cost, safety, and toxicity of this material. The manganese spinel, LiMn_2O_4 , is a low cost alternative that is safer and is more environmentally friendly. This cathode material is used in some commercial lithium ion cells. The issue with the use of this material is that the cathodes suffer from capacity fade over time. One main contribution to this capacity fading appears to result from manganese (Mn) dissolution via a disproportionation reaction of MnIII at high potentials. This dissolution can be suppressed by doping the material with other transition metals. An example of this can be seen in some interesting work on mixed metal spinels ($\text{LiNi}_{0.5}\text{Mn}_{1.5}\text{O}_4$ and $\text{LiNi}_{0.5-x}\text{Mn}_{1.5-y}\text{M}_{x+y}\text{O}_4$ $M = \text{Cr, Al, Zr}$).⁴ Raman spectroscopy was used to analyze the molecular structures of these spinels. $\text{LiNi}_{0.5}\text{Mn}_{1.5}\text{O}_4$ can be obtained in two different phases depending on the synthesis conditions. The Raman spectra from the two different phases of $\text{LiNi}_{0.5}\text{Mn}_{1.5}\text{O}_4$ are shown in Figure 1.¹ These Raman spectra were collected using a DXR 2 Raman microscope configured with a 532 nm laser. The peaks in the spectrum of the P_{432} material are sharper and stronger and the peak near 580–600 cm^{-1} (the T_{2g} peak of the spinel) is split into two compared to the single peak in the spectra of the $\text{Fd}3m$ material.⁴ The structures of the two phases have space groups corresponding to $\text{Fd}3m$ (normal spinel) and P_{432} (ordered spinel). These phases show poor contrast in the XRD but were distinguishable using Raman spectroscopy.¹ Figure 2 illustrates how different reaction conditions can lead to different phases.⁴ Doping the material with aluminum (Al) or zirconium (Zr) favors the formation of the ordered spinel structure whereas doping with chromium (Cr) favors the normal spinel structure (see Figure 3).⁴ Utilizing the differences in the Raman spectra it is also possible to evaluate the spatial distribution of phases in a sample by mapping the sample. Figure 4 shows an example of this where there are only a couple of small particles of the P_{432} phase present in a larger field of the

$\text{Fd}3m$ material.¹ The mapping data was collected using a DXR 2 Raman microscope with a motorized stage and a 532 nm laser. Thermo Scientific™ AtLus™ software allows for easy collection and analysis of Raman maps and is part of the Thermo Scientific™ OMNIC™ software used with the DXR 2 Raman microscope. The material with the ordered spinel structure (P_{432}) displays lower electrical conductivity compared to the materials with the normal spinel structure ($\text{Fd}3m$) so it is important to have an easy way to distinguish between these phases.⁴ This illustrates how the DXR 2 Raman microscope can be used for fast easy evaluation of molecular structure.

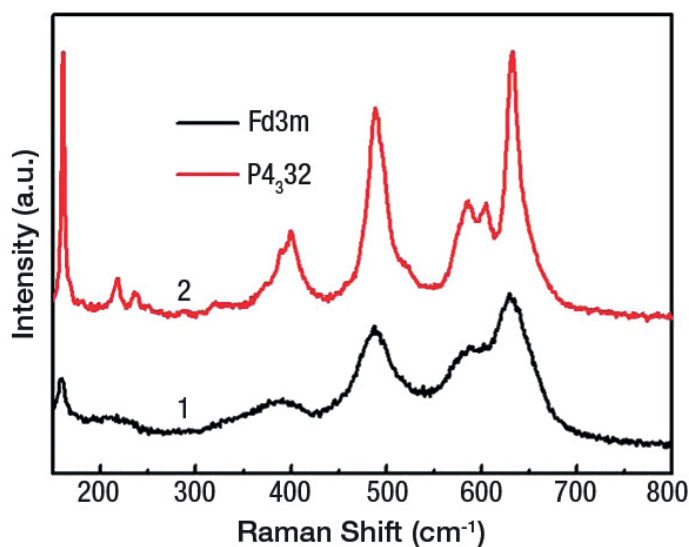


Figure 1: Raman spectra of the two phases of $\text{LiNi}_{0.5}\text{Mn}_{1.5}\text{O}_4$. Spectra were collected using a DXR 2 Raman microscope and a 532 nm laser. Adapted with permission from Xialong Zhang, Fangyi Cheng, Kai Zhang, Yanliang Liang, Siqi Yang, Jiang Liang, Jun Chen, *RSC Advances*, **2**, 2012, 5669–5675. Copyright 2012 RSC Publishing

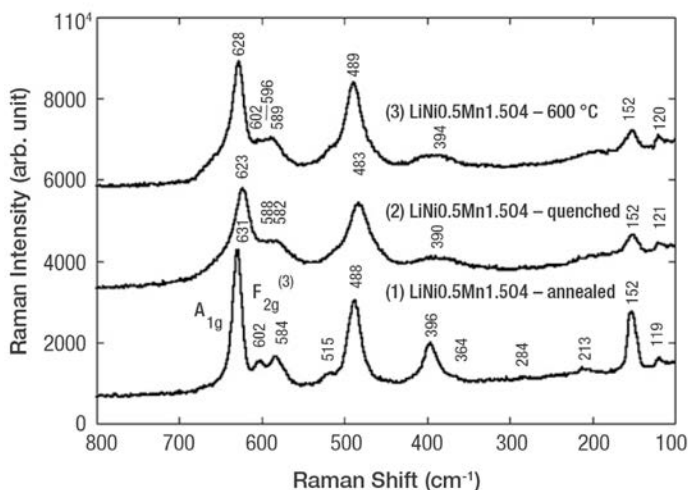


Figure 2: Raman spectra of $\text{LiNi}_{0.5}\text{Mn}_{1.5}\text{O}_4$ synthesized under various conditions. (1) Annealed at high temperature, (2) Quenched, (3) calcined at lower temperature. Spectra were collected using a Thermo Scientific™ Nicolet™ Almega™ XR dispersive Raman spectrometer equipped with a 633 nm laser. Adapted with permission from Si Hyoung Oh, Kyung Yoon Chung, Sang Hoon Jeon, Chang Sam Kim, Won Il Cho, Byung Won Cho, *J. Alloys Compd.* **469**, 2009, 244–250. Copyright 2009 Elsevier Publishing

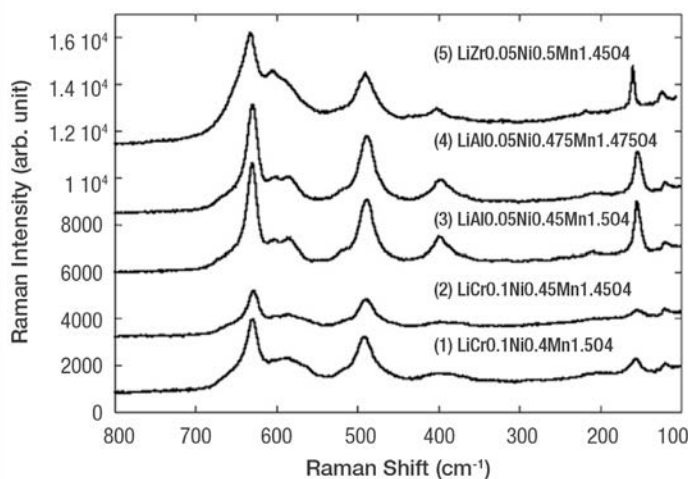


Figure 3: Raman spectra of Zr, Al, and Cr doped $\text{LiNi}_{0.5}\text{Mn}_{1.5}\text{O}_4$. (1) and (2) Cr doped (Fd3m structure); (3) and (4) Al doped ($\text{P4}_{3/2}$ structure); (5) Zr doped ($\text{P4}_{3/2}$ structure). Spectra were collected using a Nicolet Almega XR dispersive Raman spectrometer configured with a 633 nm laser. Adapted with permission from Si Hyoung Oh, Kyung Yoon Chung, Sang Hoon Jeon, Chang Sam Kim, Won Il Cho, Byung Won Cho, *J. Alloys Compd.* **469**, 2009, 244–250. Copyright 2009 Elsevier Publishing

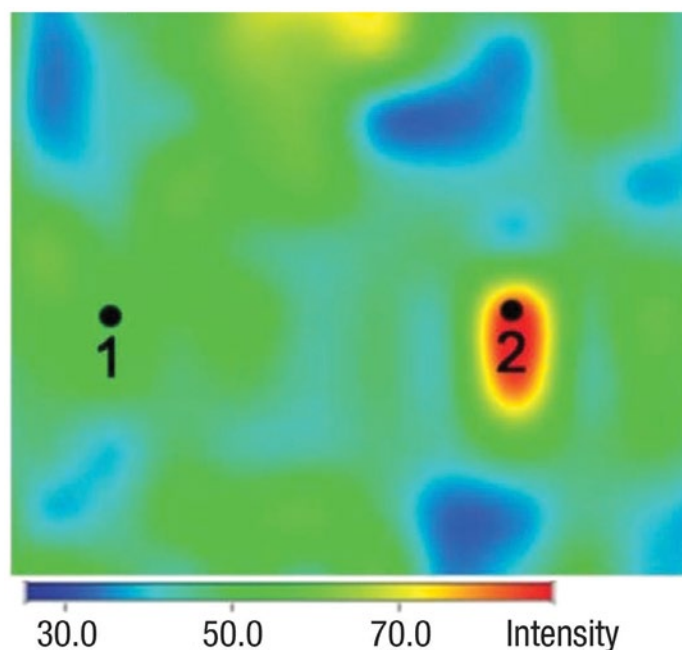


Figure 4: A Raman map showing the distribution of the two different spinel phases in a sample. The red-yellow locations (such as location 2) indicate areas of the $\text{P4}_{3/2}$ phase whereas the blue-green areas (such as location 1) represent areas of the Fd3m phase. Mapping data collected using a DXR 2 Raman microscope with a motorized stage and AtJus software. Adapted with Permission from Xialong Zhang, Fangyi Cheng, Kai Zhang, Yanliang Liang, Siqi Yang, Jiang Liang, Jun Chen, *RSC Advances*, **2**, 2012, 5669–5675. Copyright 2012 RSC Publishing

An alternative approach to doping with other transition metals is to synthesize materials with different morphologies. The approach is typically to target nanoscale materials because the smaller particles and higher surface areas tend to improve the electrochemical properties of the materials. An example of this is the report that porous nanorods of LiMn_2O_4 gave enhanced

cyclability and high-rate capacity compared to regular LiMn_2O_4 cathodes.⁵ The enhanced capacity and cycling behavior was attributed to the morphology providing short ionic diffusion distances and a structure that could more readily accommodate the lattice expansion and contraction associated with repeated lithium ion intercalation and deintercalation. A DXR 2 Raman microscope was used to confirm the spinel structure (Fd3m) of the material and was also used to monitor the stability of the material after multiple charge/ discharge cycles.⁵

Doping LiCoO_2 with other transition metals has been investigated as a way of improving cathode materials (cost, safety, performance, environmental impact). An example of this is the class of materials with the following general formula, $\text{Li}[\text{Mn}_{1-x-y}\text{Co}_x\text{Ni}_y]\text{O}_2$. Raman spectroscopy can be used to monitor the structure of these types of materials as well. It has been reported in a paper that the Raman spectra of the material changed when the lithium content increase from $\text{Li}[\text{Mn}_{0.45}\text{Co}_{0.40}\text{Ni}_{0.15}]\text{O}_2$ to $\text{Li}_{1.15}[\text{Mn}_{0.45}\text{Co}_{0.40}\text{Ni}_{0.15}]\text{O}_2$.⁶ Figure 5 shows the Raman spectra of these cathode materials.⁶ Increasing the lithium content decreased the electrostatic repulsion between adjacent layers in the structure and resulted in an increase in the Raman intensity and a shift to higher wavenumbers. The change in the Raman spectrum with lithium content illustrates the utility of Raman spectroscopy for monitoring lithium content in these types of materials.

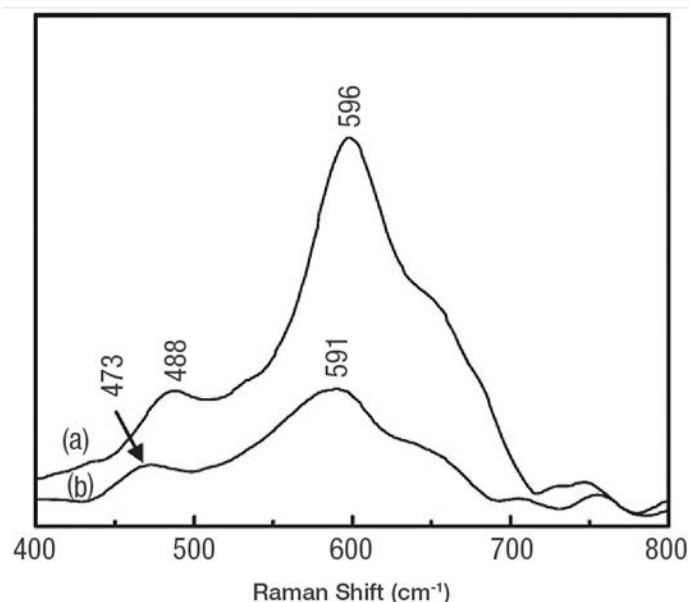


Figure 5: The Raman spectra of (a) $\text{Li}_{1.15}[\text{Mn}_{0.45}\text{Co}_{0.40}\text{Ni}_{0.15}]\text{O}_2$ and (b) $\text{Li}[\text{Mn}_{0.45}\text{Co}_{0.40}\text{Ni}_{0.15}]\text{O}_2$. Peak shift and intensity change with change in lithium content. Spectra collected using a Nicolet Almega XR dispersive Raman spectrometer configured with a 532 nm laser. Adapted with permission from Tao Wang, Zong-Huai Liu, Lihong Fan, Yinfeng Han, Xiuhua Tang, *Powder Technology*, **187**, 2008, 124–129. Copyright 2008 Elsevier Publishing

There are different ways of trying to improve the properties of cathode materials. In addition to doping and morphology changes an alternative approach is to coat the cathode with a more conductive material to form a hybrid material. This can change the solid electrolyte interface (SEI) and can improve the performance of the cathode. $\text{Li}(\text{Li}_{0.2}\text{Mn}_{0.54}\text{Co}_{0.13}\text{Mn}_{0.13})\text{O}_2$ is a member of a class of layered materials with the general form of $\text{Li}_2\text{MnO}_3 \cdot \text{LiMO}_2$ ($\text{M} = \text{Mn, Ni, Co}$). These materials have attracted attention because of high theoretical capacities up to 250 mAh/g.⁷ The problem is they have poor rate capacities and cycling behavior.

Constructing hybrid composite materials with graphene improves the cycling stability and gives enhanced high rate capacity. A DXR 2 Raman microscope fitted with a 532 nm laser was used to monitor the structure of the $\text{Li}(\text{Li}_{0.2}\text{Mn}_{0.54}\text{Co}_{0.13}\text{Mn}_{0.13})\text{O}_2$ material and provided evidence for the incorporation of graphene in the hybrid material. Peaks for both the inorganic oxide material and the graphene derived coating were observed in the Raman spectra. Figure 6 shows the Raman spectra of the cathode material before and after the reaction with graphene.⁷ The significant D band indicates substantial defects from the idealized graphene structure. There are many possible contributions to this defect peak including small domains sizes and vacancies in the graphene sheets. The existence of defects is not unexpected and in some applications can be advantageous. For instance, increased disorder in graphene anodes has been correlated with increased lithium ion capacity.⁸

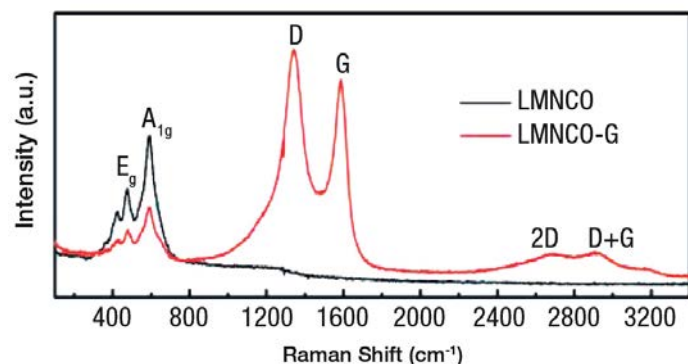


Figure 6: The Raman spectra of $\text{Li}(\text{Li}_{0.2}\text{Mn}_{0.54}\text{Co}_{0.13}\text{Mn}_{0.13})\text{O}_2$ (LMNCO) and the graphene enwrapped hybrid material (LMNCO-G). Spectra were collected using a DXR 2 Raman Microscope and a 532 nm laser. Adapted with permission from Ke-Cheng Jiang, Xing-Long Wu, Ya-Xia Yin, Jong-Sook Lee, Jaekook Kim, Yu-Guo Guo, *ACS Appl. Mater. Interfaces*, **4**(9), 2012, 4858–4863. Copyright 2012 American Chemical Society

These are just a few examples to illustrate how Raman spectroscopy can be used for the study of cathode materials. This was not meant as a comprehensive review of the literature. There are certainly other applications in the literature beyond those included here. The intent was to encourage and inspire the use of Raman spectroscopy for the analysis of battery components. Raman provides a fast and efficient way to identify materials and confirm molecular structure. It can be used on a wide variety of materials and can be used for both bulk analysis and the study of surfaces and interfaces. It has proven itself as an important analytical method for the analysis of battery components. The DXR 2 Raman microscope is a high-performance Raman microscope in an easy to use package that puts Raman spectroscopy in the reach of any user.

References

1. Xialong Zhang, Fangyi Cheng, Kai Zhang, Yanliang Liang, Siqi Yang, Jiang Liang, Jun Chen, *RSC Advances*, **2**, 2012, 5669–5675.
2. Raman Analysis of Lithium Ion Battery Components – Part II: Anodes, Thermo Scientific Application Note.
3. Raman Analysis of Lithium Ion Battery Components – Part III: Electrolytes, Thermo Scientific Application Note.
4. Si Hyoung Oh, Kyung Yoon Chung, Sang Hoon Jeon, Chang Sam Kim, Won Il Cho, Byung Won Cho, *J. Alloys Compd.* **469**, 2009, 244–250.
5. Fangyi Cheng, Hongbo Wang, Zhiqiang Zhu, Yan Wang, Tianran Zhang, Zhanliang Tao, Jun Chen, *Energy Environ. Sci.*, **4**, 2011, 3668–3675.
6. Tao Wang, Zong-Huai Liu, Lihong Fan, Yinfeng Han, Xiuhua Tang, *Powder Technology*, **187**, 2008, 124–129.
7. Ke-Cheng Jiang, Xing-Long Wu, Ya-Xia Yin, Jong-Sook Lee, Jaekook Kim, Yu-Guo Guo, *ACS Appl. Mater. Interfaces*, **4**(9), 2012, 4858–4863.
8. Timothy N. Lambert, Claudia C. Luhrs, Carlos A. Chavez, Stephen Wakeland, Michael T. Brumbach, Todd M. Alam, *Carbon*, **48**, 2010, 4081–4089.

Find out more at www.thermofisher.com/energy

ThermoFisher
SCIENTIFIC

Raman analysis of lithium-ion battery components

Part II: Anodes

Author

Robert Heintz, Ph.D., Thermo Fisher Scientific
Madison, WI, USA

Keywords

DXR 2 Microscope, anodes, carbon, graphene, lithium-ion battery, Raman

Introduction

From laptops and mobile phones to power tools and hybrid vehicles the use of portable energy storage devices is growing rapidly. As the number and types of applications expand there is a constant demand for expanding battery functionality. Different applications impose their own requirements on the technology (potential, capacity, discharge rates, charging rates, life time, operating conditions, etc.). With wide spread use there also comes greater concern with factors such as safety and environmental impact as well.

The analysis of battery components is important not only for the development of new materials but also for the study of charge/discharge mechanisms and even for confirming the quality of materials used in battery production. The complex nature of batteries requires a multifaceted combination of electrochemical analyses and materials characterization techniques. Raman spectroscopy has emerged as an important analytical technique that can be used for the characterizing of a variety of battery components. Even though a considerable amount of work has been done on the development and commercialization of lithium-ion batteries there is still considerable interest in improving the current technology and the development of new battery components. This application note will focus on examples of the analysis of anode materials for lithium-ion batteries. There are other application notes available that cover examples of the use of Raman spectroscopy for the analysis of cathode and electrolyte materials.^{1,2} The examples presented here are not meant to be an exhaustive review of the literature but are intended to illustrate the utility of Raman spectroscopy for the analysis of battery components and in particular anodic materials.



Raman spectroscopy probes molecular structure and local chemical environments and it is very useful for not only characterizing new anode materials but also for studying subtle changes in materials. The changes in the Raman spectra can be correlated with changes in the electrochemical performance of the materials. The development of easy to use but high quality Raman instruments such as the Thermo Scientific™ DXR™ 2 Raman microscope means that Raman spectroscopy can be added as a routine analytical technique to any laboratory. The DXR 2 Raman microscope is a high performance Raman spectrometer integrated with a research quality light microscope to produce a powerful molecular spectroscopy instrument for spectroscopic investigations of samples on a microscopic scale. It also includes many automated features that save time and simplify data collection and analysis without sacrificing performance. Features like SMART backgrounds and auto exposure save the user time when collecting spectra and assist with setting collection parameters. Automated alignment and calibration routines optimize instrument performance with a minimal amount of effort. These are just some of the time saving features found on the DXR 2 Raman microscope that make it easy to use and allow anyone to collect high quality Raman spectra.

One of the classical anode materials for lithium ion batteries is graphite. The Raman spectrum obtained from a graphite anode using a DXR 2 Raman microscope with a 532 nm laser is shown in Figure 1. Recently, other allotropes of Carbon besides graphite have been investigated for anode materials due to their novel physical and chemical properties. Raman spectroscopy is an excellent choice for analyzing the different allotropes of carbon (see Figure 2).³ Many of these carbon allotrope materials are strong Raman scatters and have diagnostic spectral features. Raman spectra not only can be used to distinguish different allotropes of carbon but also can provide additional information on the molecular structure.⁴ For example, Raman spectral data can be used to determine the number of sheets of graphene in a stack, it can provide information on defects and disorder in the structure of graphene, and it can be used to determine diameters of single wall carbon nanotubes.^{4,5}

Raman spectroscopy can also be used to monitor changes in anode materials during use. In one published example a DXR 2 Raman microscope was used to study the insertion of lithium into a hard carbon anode.⁶ The G band (graphite type structure) of the anode material displayed a slight shift to lower wavenumbers as the lithium insertion increased with the state of charge (SOC) of the battery. This shift has been attributed to a weakening of carbon bonds in the graphite type

structures due to negative charge transfer. This is an example of how Raman spectroscopy can be used to monitor the changes in the anode material with different states of the battery.

An active area of research is the use of carbon coatings to improve the electrochemical properties of other potential anodic materials. These carbon coatings are used to improve properties like low conductivity and cycling stability. Graphene composites have shown improved electrochemical properties. High surface area graphene improves lithium ion intercalation. Also the presence of graphene at the interfaces decreases the mechanical deterioration of anodes caused by large volume changes during cycling. One of the interesting aspects of this is that when many other applications are trending toward the fabrication of defect-free graphene, the presence of defects appears to be advantageous for anode materials. The presence of defects due to edges and vacancies in the graphene actually improves the capacity and cycling stability because it provides additional reversible storage sites for lithium ions.⁷ This means that the evaluation of defects in the graphene structures is important because it is directly related to the electrochemical properties. Raman spectroscopy can provide relative defect concentrations and this is typically expressed as the ratio of the defect peak (D band) to the graphite peak (G band) (I_D/I_G).

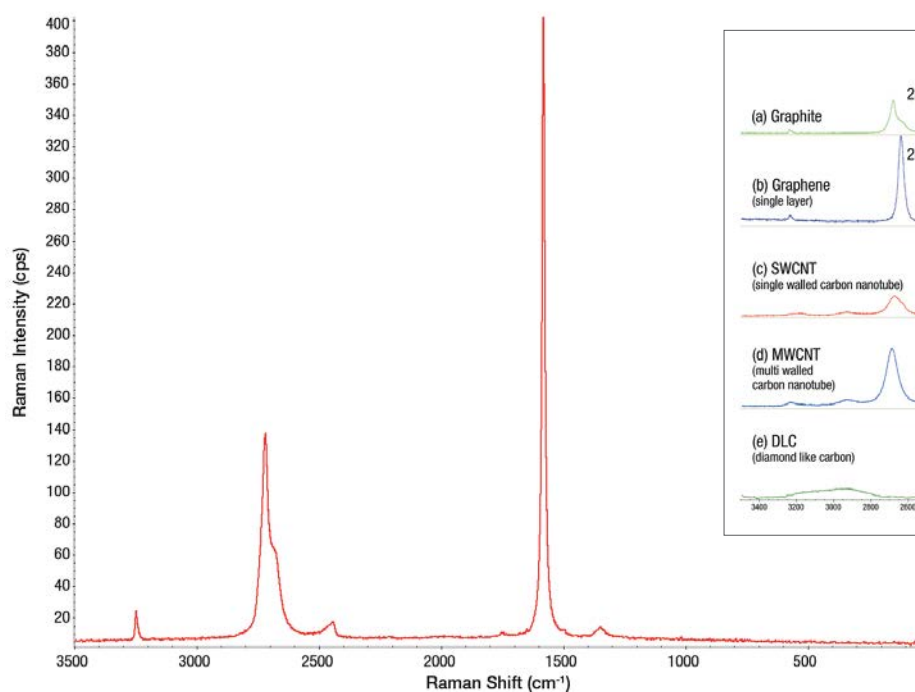


Figure 1: Raman spectrum of a graphite anode collected using a DXR 2 Raman microscope equipped with a 532 nm laser

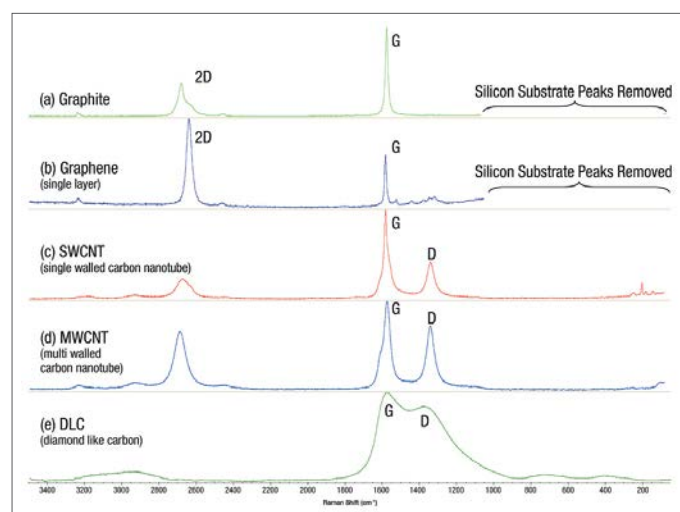


Figure 2: Raman spectra of different forms of carbon: (a) Graphite, (b) Single layer of graphene, (c) Single walled carbon nanotube (SWCNT), (d) Multi-walled carbon nanotube (MWCNT), (e) Diamond like carbon (DLC). These spectra were obtained using a DXR 2 Raman microscope and a 532 nm laser.

Silicon has been studied extensively as a promising candidate as an anode material for lithium ion batteries because of its high theoretical capacity (4200 mAh/g).⁸ However, silicon electrodes undergo a large volume expansion/contraction during cell cycling and this volume change results in mechanical degradation of the anode and a dramatic fading of capacity. The high potential capacity of the silicon anode has lead researchers to try to modify the surface of the silicon anode and thus the solid electrolyte interface (SEI) to improve the cycling behavior. One approach that has been reported is to coat the silicon anode surface with carbon using a fullerene (C60) precursor.⁹ Analysis of these thin films using a Thermo Scientific™ Nicolet™ Almega™ dispersive Raman spectrometer configured with a 633 nm laser indicated that the carbon was no longer in the fullerene form but displayed D and G bands typical of other types of carbon coatings. The G band comes from idealized graphite type carbon structures and the D band represents defects edges, vacancies, etc. from the graphite structure and can be either sp^2 or sp^3 hybridized carbon. The I_D/I_G ratio varied with the plasma power used to create the coating and with boron doping of the fullerene.^{10,11} Boron doping lowered the I_D/I_G ratio with respect to the undoped materials with similar deposition conditions. A similar approach was also carried out using diamond like carbon (DLC) films.¹² In the case of the DLC films the D and G bands overlapped significantly but they were deconvoluted into the two components. Peak fitting software like Peak Resolve in Thermo Scientific™ OMNIC™ software can be used to evaluate the relative contributions from these two types of carbon. Coating the silicon anodes with these carbon films provided more stable cycle performance along with high reversible capacity.

Tin dioxide (SnO_2) and tin disulfide (SnS_2) are both potentially useful anodic materials for lithium ion batteries. These materials are interesting because they have high theoretical capacities but like silicon they display a very large volume change during cycling and thus suffer from mechanical degradation. To address this issue, nanoscale hybrids of these materials have been investigated. In one report, nanorods of SnO_2 were combined with graphene and in another, SnS_2 nanosheets were combined with multi-walled carbon nanotubes.^{13,14} In both of these cases the hybrid materials displayed improved high rate capacities and enhanced cycling behavior.

The Raman spectrum of the SnO_2 /graphene composite material collected using a DXR 2 Raman microscope and a 532 nm laser showed both D and G bands typically associate with carbon but the G band was slightly blue shifted compared with the graphene sheet and graphene oxide peaks and this was taken as evidence of electronic interactions between the SnO_2 nanorods and the graphite type structures of the graphene sheets (see Figure 3).¹³

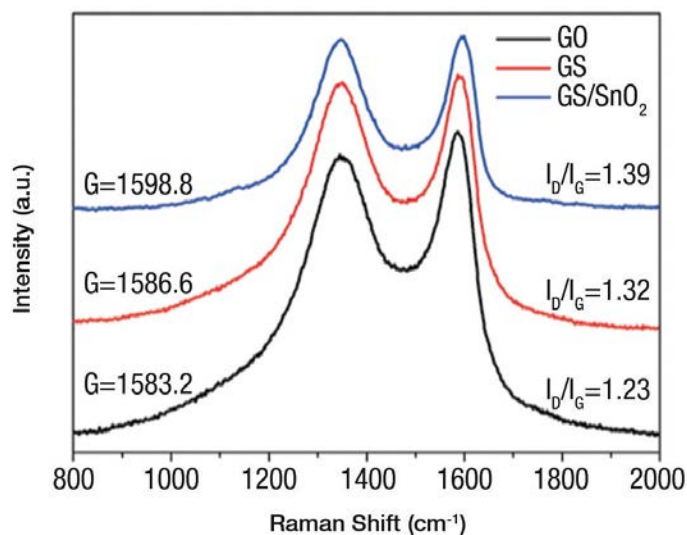


Figure 3: Hybrid anode material SnO_2 and graphene sheet (GS). Comparison of the peak location of the G band between graphene sheet (GS), graphene oxide (GO), and the hybrid anode material (GS/SnO_2). Raman spectra collected using a DXR 2 Raman microscope with a 532 nm laser. Adapted with permission from Chaohe Xu, Jing Sun, Lian Gao, *J. Mater. Chem.* **22**, 2012, 975-979. Copyright 2012 RSC Publishing

The composite material as well as the starting graphene sheet showed significant D bands indicating substantial disorder from the idealized graphene structure. This is probably not unexpected considering that the materials were prepared hydrothermally and there are many factors that could contribute to the defect concentration (small domains, vacancies, functionality, etc.)

The Raman spectra of the SnS_2 /multi-walled carbon nanotube composite anode material displayed peaks associated with nanosheets of SnS_2 (131 (w) 212 (w), 309 peak (s), 450–650 (b) cm^{-1}) as well as peaks associated with the carbon nanotubes (D and G bands) (see Figure 4).¹⁴ No peaks associated with SnS were observed despite the fact that SnS powder was used as the precursor. The SnS_2 nanosheet/MWCNT composites exhibited significantly better discharge capacities and cyclability compared to the SnS_2 nanosheets alone.

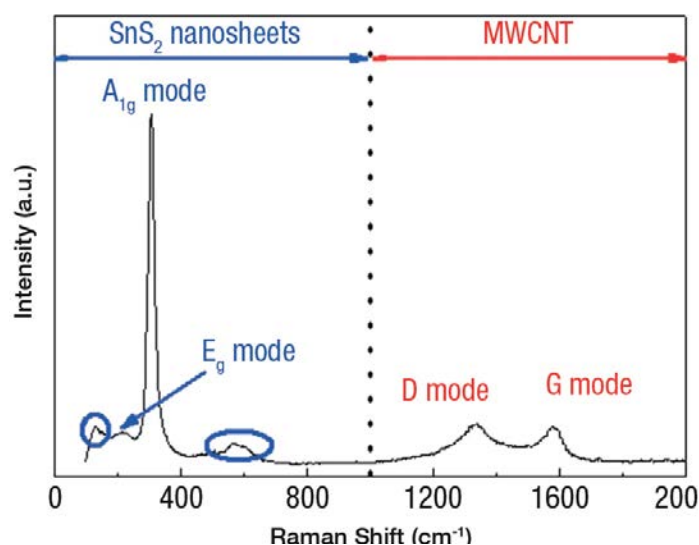


Figure 4: Raman spectrum of the SnS₂/MWCNT composite material. Peaks associated with both the SnS₂ nanosheets and the multi-walled carbon nanotubes are observed. Raman spectra collected using a Nicolet Almega dispersive Raman spectrometer. Adapted with permission from Jin-Gu Kang, Gwang-Hee Lee, Kyung-Soo Park, Sang-OK Kim, Sungjun Lee, Dong-Wan Kim, Jae-Gwan Park, *J. Mater. Chem.* **22**, 2012, 9330-9337. Copyright 2012 RSC Publishing

Lithium transition metal oxides can be used as anodes for lithium batteries as well as cathodes. Li₄Ti₅O₁₂ has the spinel structure and has been used as an anode material for lithium ion batteries. It does not have the high theoretical capacity (175 mAh/g) that materials like silicon have but it is a zero strain insertion material which means it shows only a very small change in volume during charge/discharge cycles.¹⁵ It has excellent cycle characteristics. However, it has a poor rate capacity and low conductivity. Similar approaches (morphology, doping, and coating) have been reported to improve the conductivity of Li₄Ti₅O₁₂. One example of this was detailed in a paper on how the conductivity of Li₄Ti₅O₁₂ was improved by generating a carbon composite material. Raman spectroscopy was used to confirm that the structure of the Li₄Ti₅O₁₂ was retained in the hybrid material and that carbon had been incorporated in the material (see Figure 5).¹⁵ The Raman spectra obtained using a Nicolet Almega XR dispersive Raman spectrometer with a 633 nm laser also showed the D and G bands typically associated with graphitic type carbon and disordered carbon structures were present.

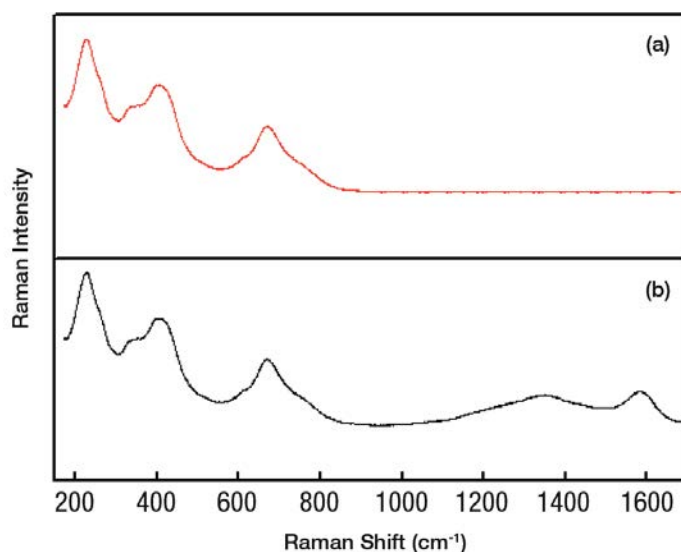


Figure 5: (a) Raman spectrum of Li₄Ti₅O₁₂ and (b) Raman spectrum of carbon coated-Li₄Ti₅O₁₂. Raman spectra were obtained using a Nicolet Almega XR dispersive Raman spectrometer configured with a 633 nm laser. Adapted with permission from Ju Bin Kim, Dong Jin Kim, Kyung Yoon Chung, Dongjin Byun, Byung Won Cho, *Phys. Scr.* **T139**, 2010. Copyright 2010 IOP Publishing

These are few examples illustrating how Raman spectroscopy can be used to analyze anode materials for lithium-ion batteries. Many anode materials involve some form of carbon and Raman spectroscopy has proven itself very useful for the analysis of carbon based materials. Not only can Raman spectroscopy be used to differentiate one form of carbon from another but it also can provide detailed structural information. However, the utility of Raman spectroscopy does not stop with carbon based materials and it can also be used to probe the structure of other materials. Transition metal oxides and tin disulfide examples were included in this application note. The versatility of use with many different types of materials and the extraordinary structural information that it can provide make Raman spectroscopy an ideal choice for the analysis of battery components. The DXR 2 Raman microscope allows for spectroscopic analysis on a microscopic scale. Advances in Raman instruments, such as the DXR 2 Raman microscope, make them easy to use while still providing high quality Raman data. Easy access to high quality Raman data is one reason for the growing number of Raman applications.

References

1. Raman Analysis of Lithium Ion battery Components – Part I: Cathodes, Thermo Scientific Application Note: 52443.
2. Raman Analysis of Lithium Ion battery Components – Part III: Electrolytes, Thermo Scientific Application Note: 52445.
3. Joe Hodkiewicz, Characterizing Carbon Materials with Raman Spectroscopy, Thermo Scientific Application Note: 51901, 2010.
4. Joe Hodkiewicz, Characterizing Graphene with Raman Spectroscopy, Thermo Scientific Application Note: 51946, 2010.
5. Joe Hodkiewicz, Technical Reference Chart for Common Calculations Involving Raman measurements with Carbon Nanomaterials, Thermo Scientific Technical Note: 51964, 2010.
6. H. Hori, M. Shikano, S. Koike, H. Sakaebe, Y. Saito, K. Tatsumi, E. Ikenaga, Abstract #117, The 15th International Meeting on Lithium Batteries, IMLB 2010, The Electrochemical Society.
7. Timothy N. Lambert, Claudia C. Luhrs, Carlos A. Chavez, Stephen Wakeland, Michael T. Brumbach, Todd M. Alam, *Carbon*, **48**, 2010, 4081-4089.
8. Arenst Andreas Arie, Joong Kee Lee, *Phys. Scr.* **T139**, 2010.
9. Arenst Andreas Arie, Wonyoung Chang, Joong Kee Lee, *J. Solid State Electrochem.* **14**, 2010, 51-56.
10. Arenst Andreas Arie, Joong Kee Lee, *J. Ceramic Processing Research*, **10 (5)**, 2009, 614-617.
11. Arenst Andreas Arie, Joong Kee Lee, *Synthetic Metals*, **161**, 2011, 158-165.
12. Sang-Ok Kim, Heung-Taek Shim, Joong Kee Lee, *J. Solid State Electrochem.* **14**, 2010, 1247-1253.
13. Chaohe Xu, Jing Sun, Lian Gao, *J. Mater. Chem.* **22**, 2012, 975-979.
14. Jin-Gu Kang, Gwang-Hee Lee, Kyung-Soo Park, Sang-Ok Kim, Sungjun Lee, Dong-Wan Kim, Jae-Gwan Park, *J. Mater. Chem.* **22**, 2012, 9330-9337.
15. Ju Bin Kim, Dong Jin Kim, Kyung Yoon Chung, Dongjin Byun, Byung Won Cho, *Phys. Scr.* **T139**, 2010.

Find out more at www.thermofisher.com/energy

ThermoFisher
S C I E N T I F I C

Raman analysis of lithium-ion battery components

Part III: Electrolytes

Author

Robert Heintz, Ph.D., Thermo Fisher Scientific
Madison, WI, USA

Keywords

DXR 2 microscope, electrolytes, lithium-ion battery, Raman Spectroscopy, Solid Polymer Electrolytes (SPE)

Introduction

Today's society is very mobile and with this comes an increasing need for portable energy sources. The demand for better battery technology continues to grow. Some applications use very small batteries and others, such as hybrid vehicles, use much larger batteries. The individual requirements (potential, capacity, discharge rate, etc.) vary with the intended use. Battery performance along with cost continue to be very important aspects of any new battery technology but factors such as safety and environmental impact are becoming increasingly important.

Electrolytes are responsible for the transport of charge in batteries. If this transport is hindered then the performance of the battery is adversely affected. Electrolytes need to be able to transport the charge efficiently but they also need to be stable under charging and discharging conditions. Side reactions of electrolytes within the battery not only reduce battery performance but shorten battery life. Improving electrolyte functionality involves not only understanding the electrolytes themselves and how they function but also how they interact with other battery components.

Lithium-ion batteries are a particularly popular battery technology that offers some of the highest energy densities and output voltages among commercial rechargeable battery systems.¹ Various lithium salts have been investigated as electrolytes. A common example of an electrolyte used in lithium ion batteries is LiPF_6 . The main issue with LiPF_6 is that it must be kept scrupulously dry to avoid hydrolysis to generate corrosive HF .² Other electrolytes such as LiAsF_6 are toxic.² Some lithium salts have low ionic conductivity (example: LiSO_3CF_3) and



some form higher resistivity barriers at the electrode surfaces (example: LiBF_4).² None of the electrolyte choices is a perfect choice so this is why the development of new electrolytes is an opportunity for improving the performance, cost, environmental impact, and safety of lithium ion batteries.

Batteries are complex devices with a variety of different components. Because of this the analysis of batteries requires a wide variety of analytical tools. The evaluation of battery components usually involves both electrochemical analysis and materials characterization methods. The various analytical techniques are often used together to provide a complimentary and comprehensive understanding of the battery components and mechanisms. Raman spectroscopy has already been established as one of the most useful and versatile analytical techniques for the analysis of a variety of different types of materials. Previous application notes have provided examples of how Raman spectroscopy can be used for the analysis of cathode and anode materials.^{3,4} Here that coverage is expanded to include examples of the analysis of electrolytes. The examples presented here are not meant to be an exhaustive review of the literature but are intended to illustrate some of the ways that Raman spectroscopy can be used and the type of information it can provide.

Commercially available Raman spectrometers have evolved into routine laboratory instruments. The Thermo Scientific™ DXR™ 2 Raman microscope is an example of this new class of Raman instruments that are easy to operate but provide high performance results. The DXR 2 Raman microscope is a fully integrated, high performance, research grade instrument that incorporates extensive automation that simplifies the collection of Raman data. For example, automated on-demand alignment and calibration present on the DXR 2 microscope eliminates time consuming manual realignment and calibration and provides an easy way to optimize instrument performance with a minimal amount of effort. This ease of use means it is much quicker to get started and provides confidence that you will get high performance and accurate results. This opens up the use of Raman spectroscopy for all types of users.

Raman spectroscopy probes molecular structure and local chemical environments. It is useful not only for the characterization of new electrolyte materials but it can also be used for studying more subtle changes in materials. For example, Raman spectroscopy can be used to study the degree of association of electrolyte ions in solutions and in polymer materials. The association of ions has a direct effect on the ion mobility and ion conductivity and thus affects battery performance.

Solid polymer electrolytes (SPE) offer some distinct advantages over electrolytes dissolved in organic solvents. In these composite materials the polymer matrix assumes the role of the solvent and lithium salts dispersed in the polymer are the electrolytes. With typical organic solvents there is a greater risk of leakage and organic based solvents can be volatile and flammable. The combination of flammable solvents and highly reactive and energetic battery components represents a potentially dangerous combination if something were to happen to the battery. Overcharging or overheating of batteries can have a disastrous effect especially with volatile solvents. The use of solid polymer electrolytes

reduces the risk of leakage and thus mitigates some what the danger of toxic, corrosive, or flammable electrolytes and solvents.⁵

The drawback of these solid polymer electrolytic systems is that they often display low ionic conductivity and poor transport of lithium ions.⁶ Poly(ethylene oxide (PEO) is an example of a polymer that is being used in solid polymer electrolytes. The low ionic conductivity of these polymer electrolytes is attributed to a crystalline phase in the polymer matrix. The low percentage of charge transfer by lithium ions is hindered because of high anion mobility. A considerable amount of research has focused on circumventing these issues.⁶

One approach to solving the issue of low ionic conductivity has been the use of additives to suppress the crystallinity of the polymer matrix and to improve the mechanical and electrochemical properties of the resulting composite polymer electrolytes. There are reports in the literature where ceramic materials such as alumina and titania have been used as fillers. For example, a Thermo Scientific™ Nicolet™ Almega™ dispersive Raman spectrometer was used to verify the phases of these materials as well as the surface modifications of the fillers (example: sulfate – SO_4^{2-}).⁷

Interesting work has been done studying additives designed to partially immobilize the anions in the polymer composite electrolytes and thus improve cation charge transfer. Raman spectroscopy was not only used to characterize the additives and the electrolytes in the polymer membranes but was also used to study the distribution of the components in the membranes. Raman mapping of the polymeric materials using a Nicolet Almega dispersive Raman spectrometer with a motorized stage and a 780 nm laser, provided images based on the Raman spectra that showed the spatial distribution of the additives and electrolytes in the polymer membranes.^{6,8} Figure 1 shows the spatial distribution of the supramolecular additive, 5,11,17,23-tetra-p-tert-butyl-25,27-bis(((N-p-nitrophenylureido) butyl) oxy)-26,28-dipropoxycalix[4]arene (Cx2), in a poly(ethylene oxide) matrix. The image is based on the ratio of a peak from the supramolecular additive (1598 cm^{-1}) to a peak associated with the PEO (840 cm^{-1}).⁹

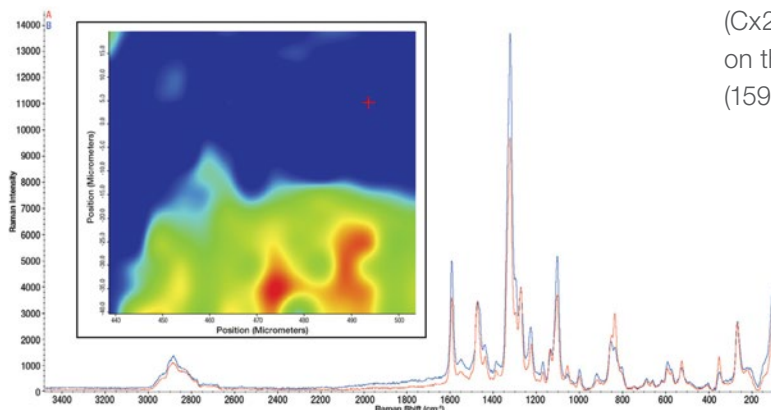
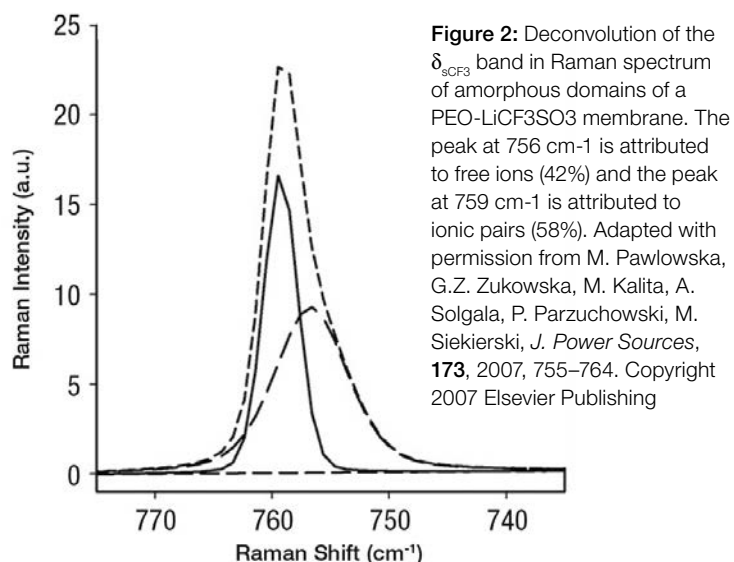


Figure 1: Spatial distribution of Cx2 in a PEO Membrane. Raman image based on the ratio of the 1600 cm^{-1} peak of Cx2 to the 840 cm^{-1} peak of PEO. Red indicates a higher concentration and blue represents a lower concentration of Cx2. The spectrum in blue comes from point B and the spectrum in red comes from point A. Mapping data was collected using a Nicolet Almega dispersive Raman spectrometer configured with a motorized stage and using a 780 nm laser. This figure was generated from data sent by the author.

The Thermo Scientific™ Atlus™ option in the Thermo Scientific™ OMNIC™ software facilitated the collection and analysis of mapping data. The red color indicates a higher concentration of additive and the blue a lower concentration. Representative spectra from each of the areas are displayed as well. The spectra are very similar but there are some differences.

Raman spectroscopy can also be used to determine the degree of association of electrolyte ions in solution. This is a very interesting application of Raman spectroscopy that is based on the fact that the degree of association of the anions (free ion, ion pairs, and triplets) has a subtle effect on the shift of the anion peaks in the Raman spectra. This is a result of slight difference in the chemical environment due to interaction with other ions.

This type of analysis was reported as part of a paper on the development of potential electrolytes for lithium ion batteries based on lithium salts of imidazole derived materials (example: lithium 4,5-dicyano-2-(pentafluoroethyl)imidazole).^{10,11} The peaks associated with CN stretching in the Raman spectra were used to evaluate the relative percentages of the various ionic associations. This was achieved by careful deconvolution and peak fitting of the composite peak. This method can be used either independently or as a compliment to methods such as the Fuoss-Kraus procedure.¹⁰ The ionic associations are of interest because the ionic conductivity is affected by the degree of association of the ions. Electrolytes with weaker associations (higher percentage of free ions) will generally display greater conductivity.



The same type of analysis can be used with other electrolytes as well. The percentages of free ions and ion pairs for lithium triflate (LiCF₃SO₃) in a PEO-LiCF₃SO₃ solid polymer electrolyte have also been determined by deconvolution and peak fitting of the CF₃ peak in the Raman spectrum of the composite material.⁸ Figure 2 shows the deconvolution of the CF₃ band of the Raman spectra into bands for the free ions and ion pairs of lithium triflate in PEO-LiCF₃SO₃.⁸ The Peak Resolve option in the OMNIC software can be used for this type of analysis.

References

1. Xialong Zhang, Fangyi Cheng, Kai Zhang, Yanliang Liang, Siqi Yang, Jing Liang, Jun Chen, *RSC Advances*, **2**, 2012, 5669–5675.
2. L. Niedzicki, M. Kasprzyk, K. Kuziak, G.Z. Zukowska, M. Marcinek, W. Wieczorek, M. Armand, *J. Power Sources*, **196**, 2011, 1368–1391.
3. Raman Analysis of Lithium Ion Battery Components – Part I: Cathodes, Thermo Scientific Application Note
4. Raman Analysis of Lithium Ion Battery Components – Part II: Anodes, Thermo Scientific Application Note
5. Jaroslaw S. Syzdek, Michel B. Armand, Pawel Falkowski, Magdalena Gizowska, Maciej Karłowicz, Lukasz Lukaszuk, Marek L. Marcinek, Aldona Zalewska, Mikolaj Szafran, Christian Masquelier, Jean M. Tarascon, Wladyslaw G. Wieczorek, Zofia G. Zukowska, *Chem.Mater.*, **23**, 2011, 1785–1797
6. Helselman, M. Kalita, A. Plewa-Marzewska, G.Z. Zukowska, E. Sasim, W. Wieczorek, M. Siekierski, *Electrochim. Acta*, **55**, 2010, 1298–1307.
7. Jaroslaw Syzdek, Michel Armand, Marek Marcinek, Aldona Zalewska, Grazyna Zukowska, Wladyslaw Wieczorek, *Electrochim. Acta*, **55**, 2010, 1314–1322.
8. M. Pawlowska, G.Z. Zukowska, M. Kalita, A. Solgala, P. Parzuchowski, M. Siekierski, *J. Power Sources*, **173**, 2007, 755–764.
9. The Raman mapping data was supplied by Dr. Grazyna Zukowska, Warsaw University of Technology, Faculty of Chemistry.
10. L. Niedzicki, M. Kasprzyk, K. Kuziak, G.Z. Zukowska, M. Armand, M. Bukowska, M. Marcinek, P. Szczecizski, W. Wieczorek, *J. Power Sources*, **192**, 2009, 612–617.
11. L. Niedzicki, G.Z. Zukowska, M. Bukowska, P. Szczecizski, S. Grugeon, S. Laruelle, M. Armand, S. Panero, B. Scrosati, M. Marcinek, W. Wieczorek, *Electrochim. Acta*, **55**, 2010, 1450–1454.

Find out more at www.thermofisher.com/energy

ThermoFisher
SCIENTIFIC

Investigate batteries with a SEM for better performance

Insights on what can be revealed on batteries structure and composition with a scanning electron microscope

The secret to improving the specifications of new generation batteries is miniaturization. SEM is an unrivaled technique for inspecting and analyzing nanoscale materials, improving production processes or detecting the reasons for failure. Get some insights into how Phenom SEMs can be used to boost the performance of your products.

The battery production cycle is a long process that involves several stages. Intermediate checks are necessary to verify the quality of the production system, starting from the inspection of raw materials, to the production of intermediate components, as well as checks on the final product, requiring the system used for the investigations to be highly versatile.

The insulating materials in batteries are, by definition, non-conductive. When imaging with a SEM, this causes an accumulation of electrons on the surface of such samples, compromising the quality of the final picture and often hiding important details. In order to flawlessly image structures of interest, different solutions are available. Reducing the vacuum level in the imaging chamber can help to discharge the sample, immediately improving image quality. The value of the current that is applied can also be altered to reduce the interactions and, when dealing with very delicate samples, prevent surface damage. If both of the previously-mentioned techniques fail, a thin layer of gold can be applied on the surface, making it conductive and ready for high resolution imaging.

The advantages of electron microscopy:

- Access to nanoscale magnification;
- Integrated, non-destructive EDS analysis to measure chemical composition of the sample locally;
- Automated routines to gather data on pores, particles and fibers - quickly and without wasting the operator's time;
- 3D reconstruction of the surface to measure morphology.

With an electron microscope, you can observe:

- Size and granulometry of powders used as raw materials;
- Size and orientation of pores and fibers in insulating membranes;
- Three-dimensional structure of electrodes after production processes;
- Response of materials to electrical or thermal solicitations;
- Presence of contaminants in the battery sublayers

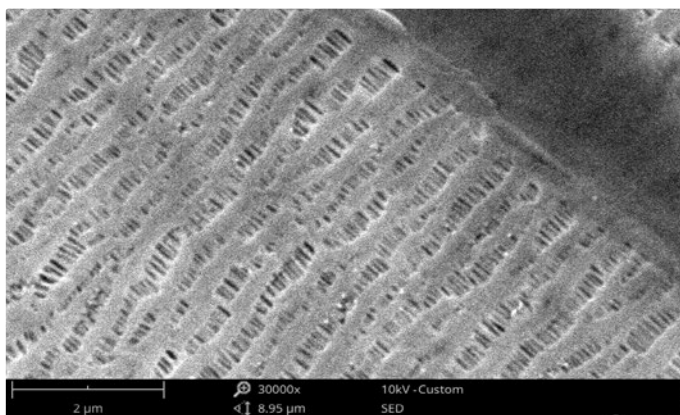


Image 1a

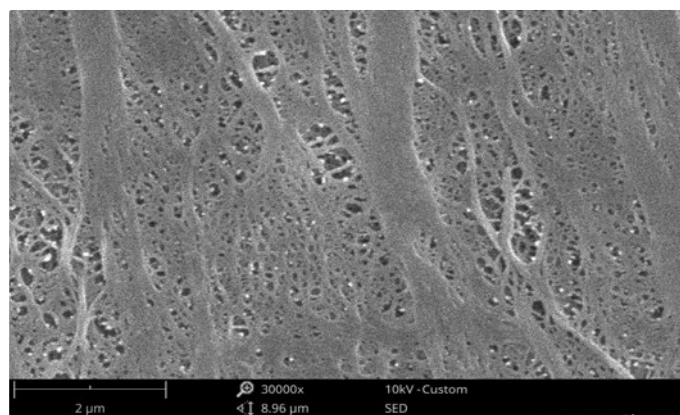


Image 1b

Image 1a and 1b: SEM images of battery insulating membranes. Highly non-conductive samples require special treatment for imaging. Operating at a different vacuum level can reduce charging effects. Coating the sample with a thin gold layer will dramatically reduce the issue.

Raw materials, such as powders, can be easily imaged at very high magnification. Particles can then be measured, to evaluate the granulometry and shape distribution within the sample. With more advanced software analysis, these measurements can be automated, providing more accurate results and saving operators a great deal of time.

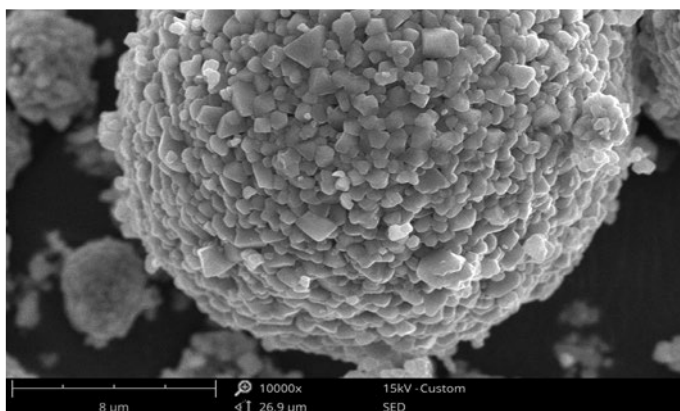


Image 2a

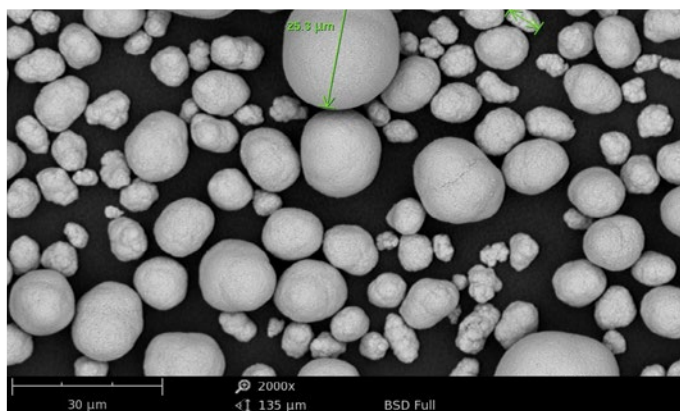


Image 2b

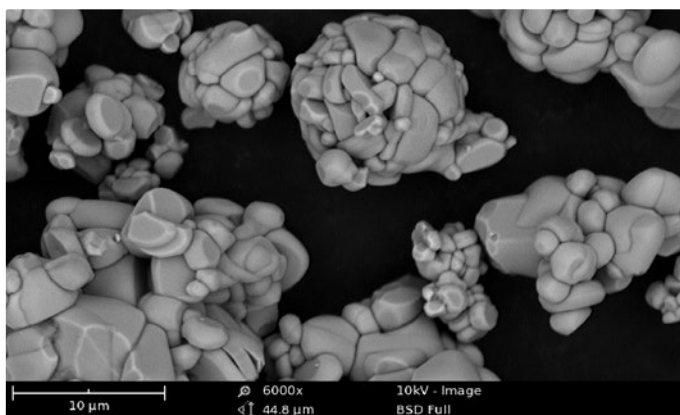


Image 2c

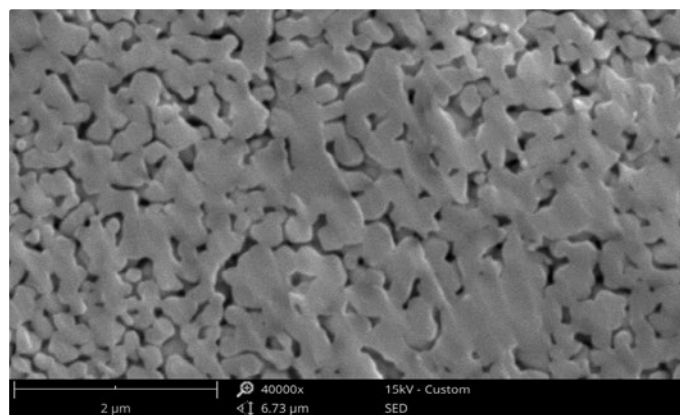


Image 2d Ion milled surface of a battery electrode. The data can be used to investigate the internal structure of the material.

Image 2a, 2b and 2c: Raw powders used in the production of cathodes. SEMs are ideal tools for investigating small particles in the range of micrometers or nanometers.

The shape and orientation of the electrodes' nanostructure is crucial to ensure that batteries have a long lasting and high efficiency. In particular, the secondary electrons detector (SED) can be used to inspect the morphology and surface topography of the sample.

With a backscattered electron detector (BSD), the image will show a different contrast for areas with different compositions. It is a formidable tool, combined with the energy-dispersive detector (EDS), in the hunt for contamination and identifying which areas to analyze.

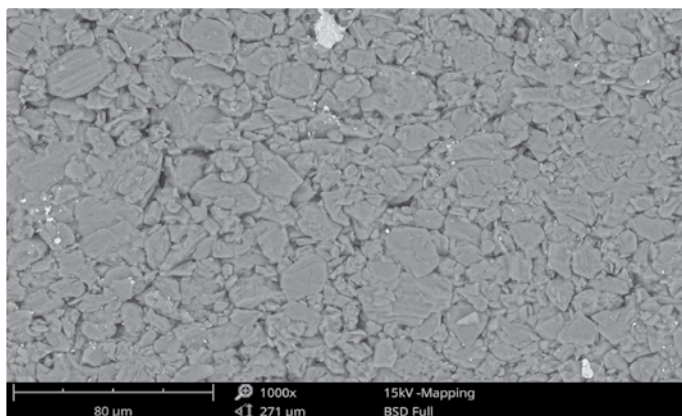


Image 3a: The structure of an electrode imaged with a BSD detector. The bright particle close to the center has a different composition compared with the rest of the sample

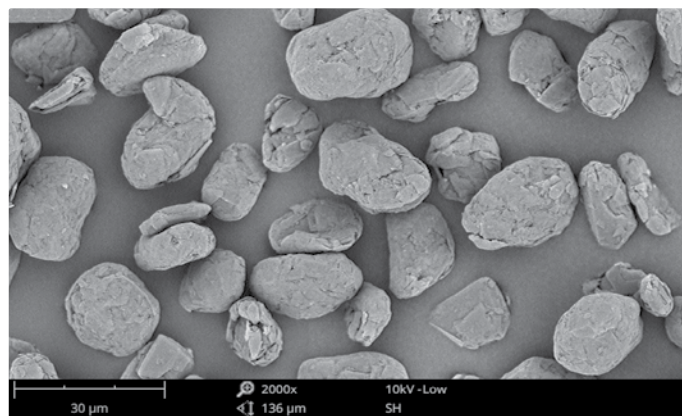


Image 3b: Powders used in the production of anodes.

Samples of interest can also be tilted and rotated, to inspect them from different points of view. *Shape from shading and stereoscopic reconstructions* can be used to create three-dimensional models of the surface and evaluate its shape and roughness.

Inspecting behavior at different temperatures, or while the sample is connected to a power supply, is also possible when using SEM. This form of testing will provide valuable information regarding the physical and chemical properties of the sample, when exposed to critical environments during its life cycle.

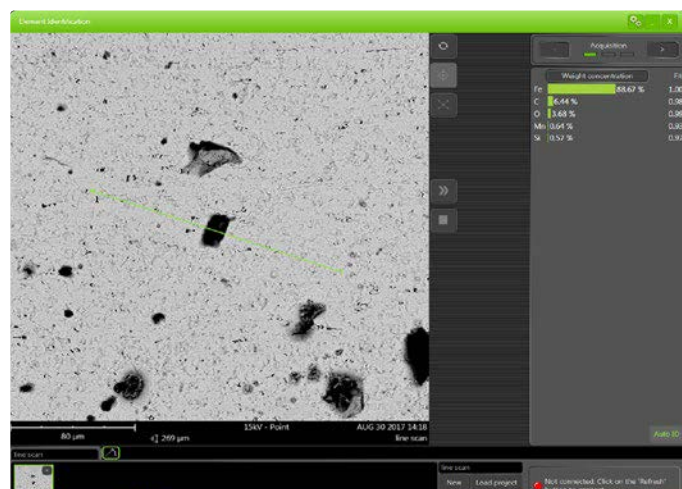


Image 4a: An example of how EDS can be used to trace how the sample composition changes along a line. Spot analysis, line scan or area map can be used to monitor the distribution of different phases in a specific region of the sample.

Find out more at thermofisher.com/phenom

ThermoFisher
SCIENTIFIC

Lithium Ion Battery Foils

Visualization of internal structure leads to improved manufacturing

A solution that implements the HeliScan microCT to visualize porosity, delamination and possible internal structural defects in Lithium Ion battery foils.

Challenge

In rechargeable lithium ion batteries, metal foil current collectors play a vital role in supporting the anode and cathode, directly influencing the batteries' performance. Improving this performance is increasingly important, as lithium-ion batteries power more and more items of our everyday life, from smartphones to electric vehicles.

An efficient and cost-effective measure to implement in any manufacturing process is to accurately identify microscopic defects in the final product. An artifact-free scanning method greatly improves this defect identification process, allowing for improvements to the manufacturing technique.

To improve the manufacturing process of lithium ion batteries, their internal structure is explored. In this example, a high-resolution scan of a large volume of the Lithium Ion battery foil sample was acquired. Typically, these samples are run on conventional micro CTs with a cylindrical acquisition method that does not allow for scanning of the sample in only one sweep. However, due to the Thermo Scientific™ HeliScan™ microCT's helical single-scan ability, it is possible to avoid such artifacts induced by stitching of multiple circular scans.

Method

The sample was cut into two smaller pieces, which were then mounted on a glass tube sample holder. To avoid damaging and/or peeling off the electrode layers, firstly $\pm 10 \times 20$ mm piece of the foil was cut off, covered from both sides with the sticky tape, followed by more precise cutting of the $\pm 2 \times 6$ mm samples. Two cathode and two anode samples were then stacked together and glued to the glass post.

Scan parameters

- Tube voltage: 60 kV
- Voxel size: 1 μm
- Scan type: Double Helix
- Total scanned volume: $2.6 \times 2.6 \times 3.6$ mm (Aspect ratio: 1.4:1)
- Scan time: 1 hour

Results

Figure 1 shows the mounting of the sample on the left, while the microCT-based visualization of the Li battery foils sample is displayed on the right.

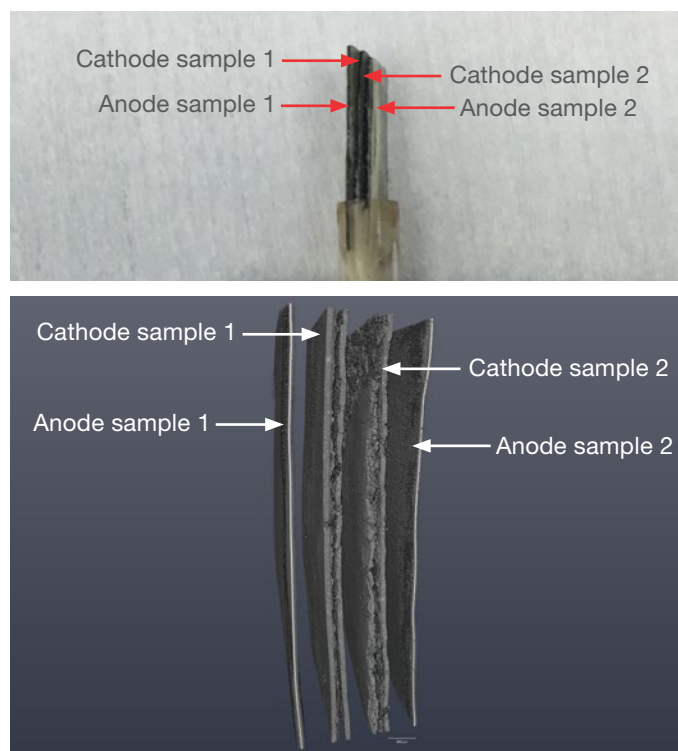


Figure 1. Digital image and microCT-based 3D visualization of the scanned anode and cathode samples.

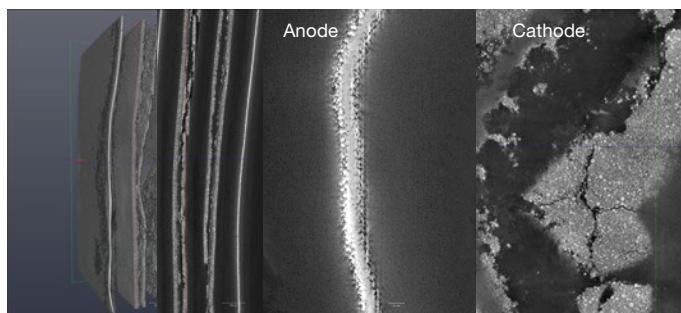


Figure 2. microCT-based 3D visualization of the Li battery foils sample.

In Figure 2, the two images on the left show the microCT-based 3D visualization of the Li battery foils sample, while the two images on the right show the microCT-based 2D visualization of the anode and cathode internal structures.

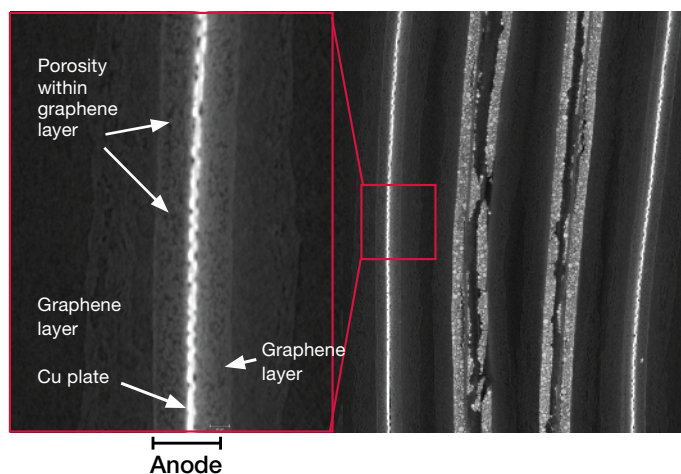


Figure 3. microCT-based 2D visualization of the anode internal structure.

Figure 3 displays the detection of porosity in graphene layers. Different components can be seen within the sample (see Figure 4). Delamination and longitudinal cracks were also visualized.

In Figure 4, the pores (voids) are shown in red while the dense particles are colored blue.

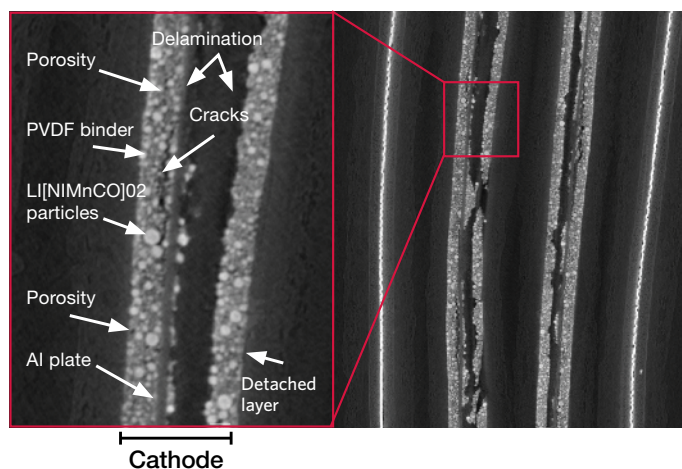


Figure 4. microCT-based 2D visualization of the cathode internal structure.

Conclusion

HeliScan microCT-based visualization of the Li battery foils revealed the internal porosity present in the anode foil, as well as the layers' delamination and unexpected longitudinal cracks within the cathode structure. The latter was not seen before; therefore, obtained results can be used for further improvement of the manufacturing process.

Sample courtesy Prof. Joachim Mayer, RWTH Aachen University.

Find out more at thermofisher.com/EM-Sales

ThermoFisher
SCIENTIFIC

Analysis of electrode materials for lithium ion batteries

Author

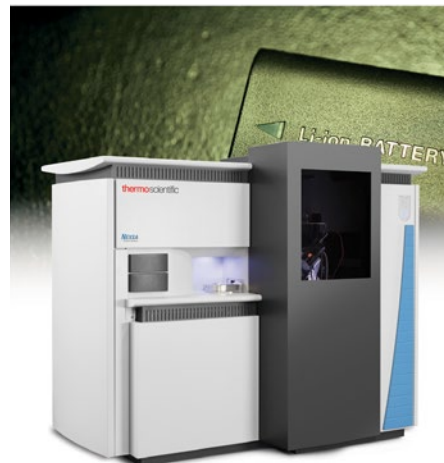
Tim Nunney
Thermo Fisher Scientific
East Grinstead, West Sussex, UK

Keywords

K-Alpha, Nexsa, air-sensitive, anode, cathode, electrodes, inert transfer, Li-ion battery, lithium, NMC, vacuum transfer

Description

The Thermo Scientific™ Nexsa™ XPS System was used to analyze the surface of lithium-ion battery electrodes. Due to the air-sensitive nature of these materials, the Nexsa vacuum transfer module was used to safely transport the samples from a glove box to the instrument without exposure to ambient atmosphere. This ensured that the surface was as representative of the electrode material as removed from the cell.



Introduction

For a large number of applications, from automobiles to portable electronics, lithium-ion battery assemblies have become the energy storage solution of choice. Lithium ion (Li-ion) battery cells are lightweight compared to other battery technology, which makes them appropriate for transport applications when combined with their relatively high energy density, and can mitigate against their higher cost. Further improving the performance of Li-ion cells, for example to increase energy density, reduce weight, decrease costs, and improve recharge times, involves developing improvements to at least one of the core components of the cell, shown in Figure 1.

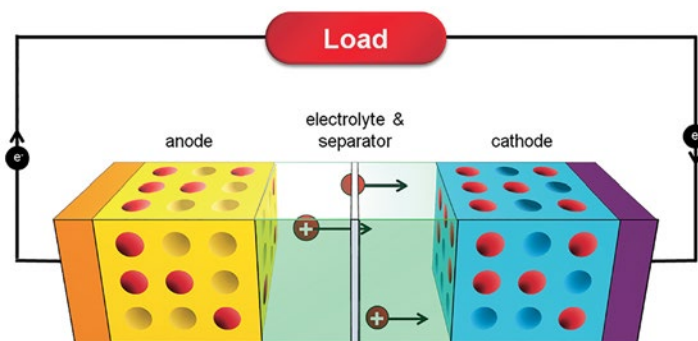


Figure 1: Li-ion cell in operation

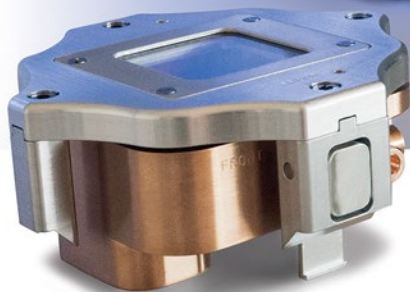
When operating, lithium stored in the anode is oxidized, and the Li^+ ions created transport through the electrolyte and separator film to the cathode. In the cathode, it is the anion that is oxidized, creating a compound that can store the arriving lithium ions. When the cell is recharged after use, the flow of ions is in the opposite direction, and they are reduced back to lithium metal to be stored in the anode. The anode is typically made from graphite, with lithium intercalated into the graphite structure. The cathode is comprised of a lithium metal oxide, the exact composition of which varies depending upon the required characteristics of the cell. The most commonly used cathode materials are LiCoO_2 (LCO – lithium-cobalt), LiMn_2O_4 (LMO – lithium-manganese), LiFePO_4 (LFP – lithium-phosphate), and $\text{Li}(\text{NiMnCo})\text{O}_2$ (NMC – nickel manganese cobalt). These oxides change in stoichiometry depending on whether the cell is charged or discharged; i.e., if the flow of Li^+ is to or from the cathode.

A by-product of the charge and discharge process is the formation of the solid-electrolyte interphase (SEI) layer on the anode. The formation and development of the SEI layer competes with the reversible lithium intercalation process, and over the lifetime of the battery the presence of the SEI will contribute to the lowering of capacity, and is a contributing factor to the ultimate failure of the cell. Understanding the SEI layer is an area of significant interest, so that it can be controlled and therefore improve cell performance. XPS depth profiling offers a way of chemically characterizing the complex mix that makes up the interphase layer, allowing an identification of the chemistries that comprise the SEI.

Method or experiment

Lithium is very sensitive to air and moisture, and so to analyze the electrode materials successfully it needs to be introduced into the XPS system without air exposure. To do this, the samples are loaded into the Vacuum Transfer Module (VTM) in a glove box. The VTM (Figure 2), compatible with the K-Alpha and Nexsa instruments, is evacuated in the glove box antechamber, and then transported to the XPS system. As the VTM is held together by air pressure, it automatically opens during the pump-down cycle in the system load-lock and is therefore integrated into the standard, automated, sample transfer process.

Figure 2: The vacuum transfer module allows samples that have been prepared in an inert environment to be transferred into the spectrometer chamber without exposure to air.



In these experiments, two cathode samples were investigated. One sample was a pristine, unused sample; the other sample was from a cell that had been through several chargedischarge cycles, and was in a charged state when the cell was disassembled.

Results

Survey spectra collected from the as received cathode samples are shown in Figure 3. The cathode material is $\text{Li}(\text{Ni}_x\text{Mn}_y\text{Co}_z)\text{O}_2$, prepared using a binder medium to hold the material together. The binder is a mixture of fluorine and oxygen containing polymers, and for the pristine sample is evident as a significant amount of residue on the surface. This could be important during the first use of the cathode, if the binder residue is mobile in the electrolyte, or reacts to begin the formation of a surface layer which impedes ion transport.

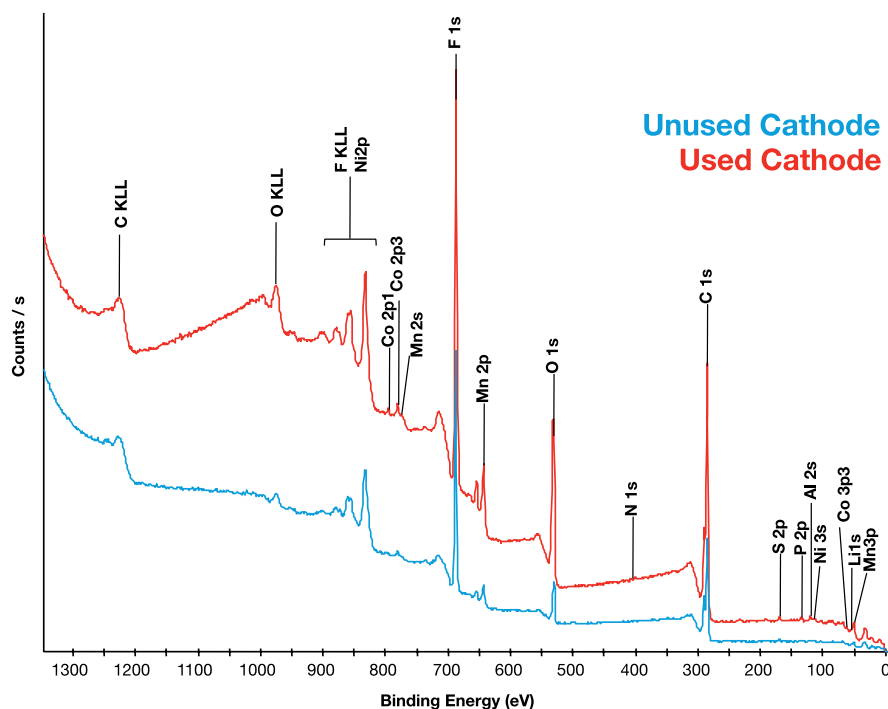


Figure 3: Survey spectra from pristine cathode (blue) and cycled cathode (red) samples

The cycled cathode still shows the presence of the binder, and also evidence of residue from the electrolyte at the surface. Figure 4 shows the variation in the NMC components of the two samples (excluding oxygen). The relative intensities of the Ni, Mn, and Co components are very similar between the two samples, but the amount of Li detected is around 40% of that seen in the pristine cathode. This is as expected in a sample from a charged cell, where the Li ion transport has been towards the anode and away from the cathode, resulting in a depleted level of lithium in the cathode.

Summary

By using the vacuum transfer module and the Nexsa XPS System it is possible to analyze Li-ion battery components. Analysis of unused and cycled cathode samples determined the expected variation in lithium content.

Acknowledgements

We would like to thank Dr. Harry Meyer III (HTML, Oak Ridge National Lab., TN, USA), Dr. David Wood III, and Dr. Debasish Mohanty (NTRL, Oak Ridge National Lab., TN, USA) for the supply of samples, facilities and help with this analysis.

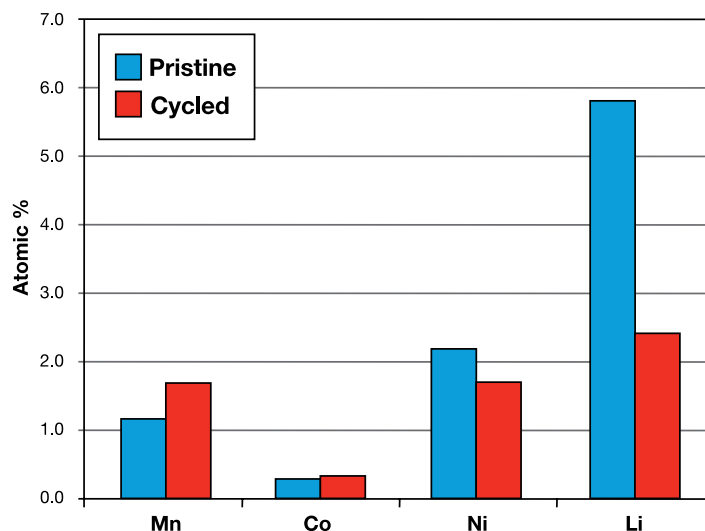


Figure 4: Composition variation for the NMC components

Determination of Tetrafluoroborate, Perchlorate, and Hexafluorophosphate in a Simulated Electrolyte Sample from Lithium Ion Battery Production

Authors

Thunyarat Phesatcha,¹ Suparerk Tukkeeree,¹ Jeff Rohrer²
¹Thermo Fisher Scientific, Bangkok, Thailand; ²Thermo Fisher Scientific, Sunnyvale, CA, USA

Introduction

Lithium ion batteries are commonly used in portable consumer electronic devices. The electrolyte solution in these batteries consists of a lithium salt in an organic solvent. Commonly used salts are lithium hexafluorophosphate (LiPF₆), lithium perchlorate (LiClO₄), lithium tetrafluoroborate (LiBF₄), lithium hexafluoroarsenate (LiAsF₆), lithium hexafluoroarsenate (LiSiF₆), and lithium tetraphenylborate (LiB(C₆H₅)₄). Some organic solvents used in the electrolyte solution are ethylene carbonate, diethyl carbonate, dimethyl carbonate, ethyl methyl carbonate, propylene carbonate, methyl formate, methyl acrylate, methyl butylate, and ethyl acetate. The electrolyte in lithium batteries may have a mixture of these lithium salts and organic solvents. The electrolyte's concentration in the solvent ranges from 0.1 to 2 mol/L, with an optimal range of 0.8–1.2 mol/L. The anions of the added lithium salts can be determined by ion chromatography (IC) to ensure that the solutions have been prepared at the proper concentrations.

Here, the authors prepare simulated samples that contain either lithium tetrafluoroborate, lithium perchlorate, or lithium hexafluorophosphate in an equal mixture of ethylene carbonate, diethyl carbonate, and propylene carbonate, and demonstrate that the anionic content can be determined accurately using a Reagent-Free™ IC (RFIC™) system. The RFIC system allows the analyst to avoid the problems encountered in eluent preparation. The RFIC system also delivers excellent retention time reproducibility for easy and reproducible quantification in the analysis of lithium ion battery electrolyte solutions.

Equipment

- Thermo Scientific™ Dionex™ ICS-3000* system:
 - DP Dual Pump
 - DC Detector/Chromatography module with dual-temperature zone equipped with 6-port valve
- EG Eluent Generator module
- Thermo Scientific™ Dionex™ Chromeleon™ Chromatography Data System software Version 6.80 SR7

Reagents and Standards

- Deionized water (DI), Type I reagent grade, 18 MΩ-cm resistivity or better
- Lithium tetrafluoroborate (LiBF₄, Sigma-Aldrich)
- Lithium perchlorate (LiClO₄, Sigma-Aldrich)
- Lithium hexafluorophosphate (LiPF₆, Sigma-Aldrich)
- Ethylene carbonate, 98% (C₃H₄O₃, Sigma-Aldrich)
- Diethyl carbonate, 99% (C₅H₁₀O₃, Sigma-Aldrich)
- Propylene carbonate (C₄H₆O₃, Sigma-Aldrich)

Chromatographic Conditions

Columns:	Thermo Scientific™ Dionex™ IonPac™ AS20, 4 × 250 mm (P/N 063148)
Guard:	Dionex IonPac AG20, 4 × 50 mm (P/N 063154)
Eluent Source:	Thermo Scientific™ Dionex™ EluGen™ EGC II KOH Column (P/N 058900) with Thermo Scientific™ Dionex™ CR-ATC Continuously Regenerated Anion Trap Column (P/N 060477)
Gradient Steps:	Potassium hydroxide; 15 mM from –7 to 10 min 15 to 80 mM (Curve 4) from 10 to 13 min and 80 mM from 13 to 26 min
Flow Rate:	1.2 mL/min
Sample Volume:	10 µL
Column Oven:	35 °C
Pressure:	~2200 psi
Detection:	Suppressed conductivity, Thermo Scientific™ Dionex™ ASRS™ 300 Anion Self-Regenerating Suppressor, 4 mm (P/N 060554) Thermo Scientific™ Dionex™ CRD 200 Carbonate Removal Device, 4 mm (P/N 062983), Recycle mode
Suppressor Current:	238 mA

*This application can be conducted with any Dionex RFIC system.

Preparation of Solutions and Reagents

Stock Standard Solutions

Dissolve 0.093, 0.112, and 0.105 g of lithium tetrafluoroborate, lithium perchlorate, and lithium hexafluorophosphate, respectively, in DI water in separate 100 mL volumetric flasks. Dilute to volume with DI water.

Calibration Standard Solutions

Prepare mixed calibration standard solutions by diluting a mixture of defined volumes of 1000 mg/L stock standard solutions with DI water in a 10 mL volumetric flask. The volumes of each 1000 mg/L stock standard solution and the prepared calibration standard concentrations are shown in Table 1.

Concentration of each Anion (mg/L)	Volume of each 1000 mg/L Stock Standard Solution (μL)	Final Volume (mL)
5	50	10
10	100	10
20	200	10

Table 1. Volumes of 1000 mg/L stock standard solutions used to prepare calibration standards at the listed concentrations.

Eluent

The eluent generator (EG) produces the eluent using the Dionex EluGen EGC II KOH cartridge and DI water (18 MΩ-cm resistivity or better) supplied by the pump. The eluent concentration is controlled by the Chromeleon Chromatography Data System software. The Dionex EluGen cartridge requires at least 14 MPa (2000 psi) of system backpressure, which ensures optimal removal of electrolysis gas from the eluent produced by the generator. See the Dionex ICS-3000 Operator's Manual (Document No. 065031-04) for instructions on adding backpressure.

Mixture of Three Carbonate Solvents (1:1:1)

Thoroughly mix 10 g each of ethylene carbonate, diethyl carbonate, and propylene carbonate.

Simulated Electrolyte Sample

To simulate samples from lithium ion batteries, prepare three samples. Two samples are 1 M solutions of lithium tetrafluoroborate and lithium perchlorate prepared in the mixture of three carbonate solvents. The third sample is a 1 M solution of lithium hexafluorophosphate prepared in DI water. Later, this sample will be diluted 1:1 with the mixture of three carbonate solvents. This preparation is necessary because lithium hexafluorophosphate does not dissolve in the mixture of three carbonate solvents. Table 2 shows details of the sample preparation for these three samples.

Simulated Sample	Weight of Lithium Salt (g)	Solvent	Final Volume (mL)
1 M lithium tetrafluoroborate	0.938	Mixture of three carbonate solvents	10
1 M lithium perchlorate	1.068	Mixture of three carbonate solvents	10
1 M lithium hexafluorophosphate	1.519	DI water	10

Table 2. Preparation of simulated samples.

Sample Preparation

Tetrafluoroborate and Perchlorate Sample

Dilute 1 M lithium tetrafluoroborate and lithium perchlorate solutions 10,000 times with DI water.

Hexafluorophosphate Sample

Mix 1 M lithium hexafluorophosphate with the mixture of three carbonate solvents in a 1:1 ratio. Dilute this solution 5,000 times with DI water.

Results and Discussion

Chromatography

The analyte anions in this application—perchlorate, tetrafluoroborate, and hexafluorophosphate—are classified as polarizable anions. These anions tend to be strongly retained and have poor peak shapes with typical anion-exchange columns. With anion-exchange columns, analysts often include organic additives in the eluent (for example, p-cyanophenol) to improve the peak shapes of polarizable anions. This is undesirable because it increases eluent costs, eluent complexity, waste disposal costs, and decreases detection sensitivity. To address this problem, we designed the Dionex IonPac AS16 column and later, the IonPac AS20 column. These are high-capacity, hydroxide-selective, anion-exchange columns designed for polarizable anions. The stationary phases in these columns allow easy elution of polarizable anions with good peak shapes while requiring no organic solvent in the eluent. The high capacity allows the determination of polarizable anions in the presence of high concentrations of other anions.

In the analysis presented here, the authors used the Dionex IonPac AS20 column because it has higher column capacity than the AS16 column (310 µeq/column compared to 160); however, the AS16 column can also be used with different hydroxide eluent concentrations. Because both columns can be used with hydroxide eluents, they can be paired with an eluent generator (EG). An EG, the key component of an RFIC system, produces error-free pure hydroxide eluent. This translates to highly reproducible analyte retention times for reproducible determination without the labor involved in manually preparing hydroxide eluents. Figure 1 shows the separation of three mixed standard solutions (used for method calibration) of the three analytes of interest: perchlorate, tetrafluoroborate, and hexafluorophosphate. The three anions were well separated in about 25 min, with the first analyte, tetrafluoroborate, eluting at about 13 min. The first 12 min of the separation were included to allow most common inorganic anions to elute so that they did not interfere with the determination of the three analytes. Tetrafluoroborate eluted between sulfate and phosphate, while perchlorate and hexafluorophosphate eluted after phosphate. Table 3 shows the calibration information for each analyte.

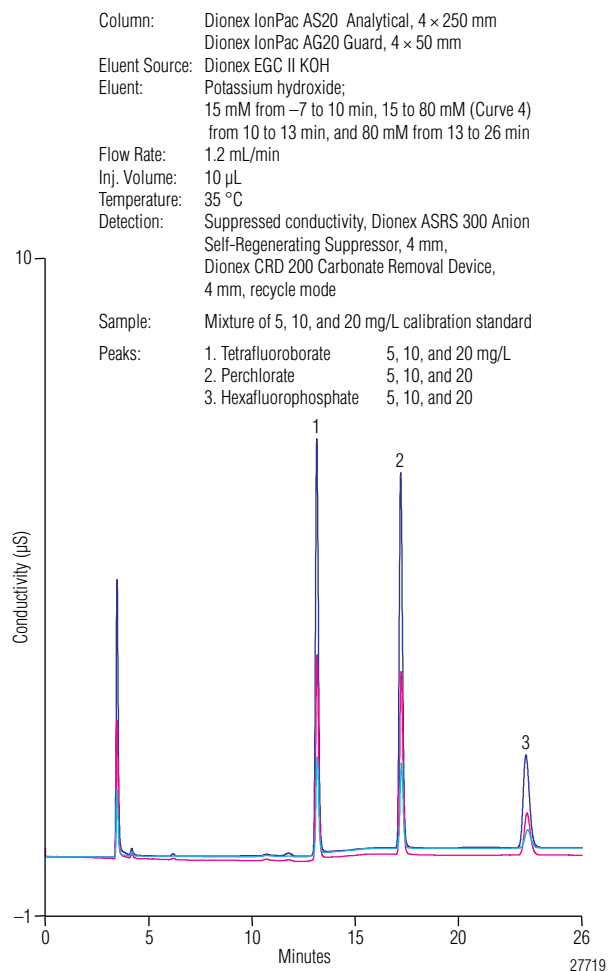


Figure 1. Overlay of chromatograms of the calibration standards.

Analyte	Concentration (mg/L)				Result	
	Level 1	Level 2	Level 3	% Coeff.Det.	Offset (µS*min)	Slope (µS*min)/mg/L
Tetrafluoroborate	5	10	20	100.00	–0.0485	0.0606
Perchlorate	5	10	20	99.99	–0.0597	0.0623
Hexafluorophosphate	5	10	20	99.91	–0.0449	0.0296

Table 3. Concentrations of calibration standards and the calibration results reported by the Chromeleon software.

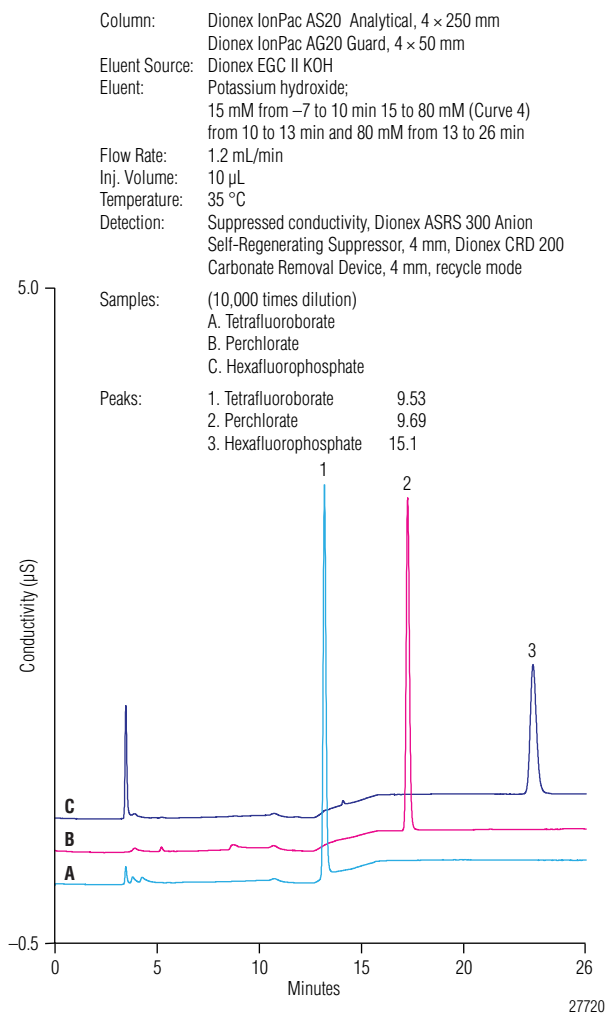
Sample Analysis

Here, three simulated lithium ion battery electrolyte samples were prepared. One molar solution each of lithium tetrafluoroborate and lithium perchlorate was prepared in a mixture of three carbonate solvents. One molar lithium hexafluorophosphate was prepared in DI water and then diluted 1:1 with the mixture of three carbonate solvents. The first two samples were diluted

1 to 10,000 and the third sample was diluted 1:5,000 with DI water prior to analysis by IC. Figure 2 shows the chromatography of each of the three samples. The Dionex CRD 200 Carbonate Removal Device was used to eliminate any possible interference from sample carbonate. Short-term reproducibility was measured by making five injections of each sample. The data in Table 4 show good reproducibility for the amount measured in each sample. To judge accuracy, the authors compared measured concentration to the calculated concentration (Table 5) and found that the measured concentration was between 97.4, 104, and 109% of the calculated concentration for perchlorate, hexafluorophosphate, and tetrafluoroborate, respectively. As a second test of accuracy, the simulated samples were spiked with 2 mg/L of the same anion prior to dilution. The data in Table 5 also show good recoveries for each anion, suggesting method accuracy.

Conclusion

This application demonstrates an IC method that uses an RFIC system to easily assay the anions in the simulated lithium ion battery electrolyte samples. The results show that this method is both accurate and reproducible.



Injection No.	Amount (mg/L)					
	Tetrafluoroborate		Perchlorate		Hexafluorophosphate	
	Sample	Spiked Sample	Sample	Spiked Sample	Sample	Spiked Sample
1	9.57	11.3	9.74	11.9	15.1	16.7
2	9.45	11.3	9.68	11.9	15.1	16.8
3	9.58	11.1	9.75	11.7	15.1	16.7
4	9.55	11.3	9.69	11.8	15.1	16.8
5	9.48	11.2	9.57	11.8	15.2	16.8
Average	9.53	11.3	9.69	11.8	15.1	16.8
RSD	0.62	0.55	0.74	0.64	0.30	0.26

Table 4. Assay results for the samples and spiked samples.

Ion	Calculated Concentration after 10,000 Times Dilution (mg/L)	Average Found Concentration (mg/L)	Recovery (%)	Spiked Concentration (mg/L)	Average Found Concentration in Spiked Sample (mg/L)	Recovery (%)
Tetrafluoroborate	8.70	9.53	109	2	11.3	88.5
Perchlorate	9.95	9.69	97.4	2	11.8	106
Hexafluorophosphate	14.5	15.1	104	2	16.8	85.0

Table 5. Assay results for the samples and spiked samples.

Find out more at thermofisher.com/dionex

ThermoFisher
S C I E N T I F I C

Determination of Dissolved Manganese in Lithium/Manganese Oxide Battery Electrolyte

Authors

Chanita Chantarasukon,¹ Suparerk Tukkeeree,¹ and Jeff Rohrer²
¹Thermo Fisher Scientific, Bangkok, Thailand; ²Thermo Fisher Scientific, Sunnyvale, CA USA

Key Words

Lithium-Ion Battery, Cathode, Dionex IonPac CS12A Column, Reagent-Free Ion Chromatography System

Introduction

Lithium-ion batteries are widely used in products such as portable consumer electronic devices and electric vehicles. Many different materials are used to make the cathode in lithium batteries, including those that are manganese-, cobalt-, and nickel-based. Lithium-ion batteries that are manganese-based are more environmentally friendly, have a good safety record, and can be made at a lower cost; however, they have a shorter lifetime than other types of lithium-ion batteries. One of the reported causes of lifetime loss is the dissolution of manganese from the cathode into the electrolyte during cycling (i.e., charging/discharging). Lithium/lithium manganese oxide ($\text{Li/LiMn}_2\text{O}_4$) is a type of battery that has a manganese-based cathode.

In Thermo Scientific Application Note (AN) 258, ion chromatography (IC) was applied to determine the anions tetrafluoroborate, perchlorate, and hexafluorophosphate in a simulated electrolyte solution for lithium-ion batteries.¹ AN 258 used a Reagent-Free™ IC (RFIC™) system, and it is also possible to use an RFIC system to determine manganese in a simulated electrolyte solution for lithium-ion batteries. There is one report of an IC method that uses manually prepared eluents and direct conductivity detection to determine dissolved manganese in the electrolyte of a $\text{Li/LiMn}_2\text{O}_4$ battery.² However, that method has poor sensitivity, which is inherent with direct conductivity detection. Even with a three-component (tartaric acid, dipicolinic acid, and ascorbic acid) mobile phase, the manganese peak exhibits extreme tailing on the chosen column. A better IC cation column will improve peak shape and therefore improve integration precision and method accuracy, while suppressed conductivity detection will improve method sensitivity.



The work shown here uses an RFIC system with suppressed conductivity detection to quantify dissolved manganese in the simulated electrolyte of a $\text{Li/LiMn}_2\text{O}_4$ battery. The method uses the Thermo Scientific™ Dionex™ IonPac™ CS12A column set, which was designed to deliver good peak shapes for cations such as manganese(II) (Mn^{2+}), with a simple methanesulfonic acid (MSA) eluent produced by an eluent generator. The combination of the RFIC system and a quality IC column yields a method that is sensitive, accurate, reproducible, and easy to execute, requiring only the addition of deionized water to the RFIC system.

Goal

To develop an IC method that accurately determines dissolved manganese in the electrolyte of a $\text{Li/LiMn}_2\text{O}_4$ battery using an RFIC system

Equipment

- Thermo Scientific Dionex ICS-2100 Integrated RFIC system,* including a Thermo Scientific Dionex AS-AP Autosampler
- Thermo Scientific™ Dionex™ Chromeleon™ Chromatography Data System (CDS) software version 6.80, SR9 or higher

*Any Thermo Scientific RFIC system may be used.

Reagents and Standards

- Deionized (DI) water (H₂O), Type I reagent grade, 18 MΩ-cm resistivity or better
- Ethylene Carbonate (C₂H₄O₃), 99% (Fisher Scientific P/N 50-700-5617)
- Ethyl Methyl Carbonate (C₄H₈O₃), 99% (Sigma-Aldrich® P/N 754935)
- Vinylene Carbonate (C₃H₂O₃), 97% (Fisher Scientific P/N 50-751-1840)
- Lithium Hexafluorophosphate (LiPF₆), 98% (Fisher Scientific P/N 21324-40-3)
- Manganese(II) Sulfate, Monohydrate (MnSO₄·H₂O) (Fisher Scientific P/N 10034-96-5)

Preparation of Solutions and Reagents

Mixture of Ethylene Carbonate and Ethyl Methyl Carbonate, 1:1 (w/v)

Dissolve 10 g of ethylene carbonate in 10 mL of ethyl methyl carbonate.

Manganese Stock Standard Solution, 1000 mg/L

Place 0.308 g of manganese(II) sulfate monohydrate in a 100 mL volumetric flask, dissolve in DI water, bring to volume with DI water, and mix.

Working standard solution

Add the appropriate volumes of 1000 mg/L manganese stock standard solution into separate 100 mL volumetric flasks, bring to volume with DI water, and mix. The volumes of manganese stock standard solution used for the preparation of working standard solutions are shown in Table 1.

Level	Volume of Manganese Stock Solution (1000 mg/L) Used for a 100 mL Preparation (mL)	Concentration (mg/L)
1	0.010	0.10
2	0.020	0.20
3	0.040	0.40
4	0.080	0.80
5	0.100	1.00

Table 1. Preparation of working standards.

Sample Preparation

Preparation of a Simulated Sample

Prepare 1.12 M of LiPF₆ and 2 wt % of vinylene carbonate in the mixture of ethylene carbonate and ethyl methyl carbonate by placing 1.7 g of LiPF₆ and 0.2 g of vinylene carbonate in a 10 mL volumetric flask; dissolve, then bring to volume with the mixture of ethylene carbonate and ethyl methyl carbonate. Prepare a 1 to 50 dilution of this simulated sample using DI water prior to injection. This is the same dilution used in the published method.²

Spiked Sample Simulation

Prepare 5 mg/L of manganese, 1.12 M of LiPF₆, and 2 wt % of vinylene carbonate in the mixture of ethylene carbonate and ethyl methyl carbonate by placing 1.7 g of LiPF₆, 0.2 g of vinylene carbonate, and 50 µL of 1000 mg/L manganese stock standard solution in a 10 mL volumetric flask; dissolve, then bring to volume with the mixture of ethylene carbonate and ethyl methyl carbonate. Prepare a 1 to 50 dilution of this spiked simulated sample using DI water prior to injection.

Chromatographic Conditions

Columns:	Dionex IonPac CG12A Guard, 4 × 50 mm (P/N 046074) Dionex IonPac CS12A Analytical, 4 × 250 mm (P/N 046073)
Eluent Source:	Thermo Scientific Dionex EGC III MSA Eluent Generator Cartridge (P/N 074535) with Thermo Scientific Dionex CR-CTC II Continuously Regenerated Cation Trap Column (P/N 066262)
Eluent Concentration:	20 mM MSA
Flow Rate:	1.0 mL/min
Inj. Volume:	20 µL
Temperature:	35 °C
Detection:	Suppressed Conductivity, Thermo Scientific™ Dionex™ CSRS™ 300 Cation Self-Regenerating Suppressor, 4 mm (P/N 064556), Recycle Mode, Current 60 mA
Total Conductivity:	~0.34 µS

Analyte	Concentration (mg/L)					Calibration Results			
	Level 1	Level 2	Level 3	Level 4	Level 5	Points	r ²	Offset	Slope
Manganese	0.1	0.2	0.4	0.8	1.0	15	0.9997	-0.0046	0.1617

Table 2. Working standard concentrations and calibration results.

Results and Discussion

Separation

Manganese is a divalent cation that can be separated from six common cations using the Dionex IonPac CS12A column set with isocratic elution. As shown in Figure 1, manganese is well separated from the other common divalent cations—magnesium and calcium—using a 20 mM MSA eluent. Figure 1 also shows that manganese is well resolved from other common cations. Note the good peak shape for manganese and the other cations. The MSA eluent is automatically produced by pumping DI water through the eluent generator cartridge with the concentration controlled by Chromeleon CDS software.

Method Calibration

The method was calibrated before sample analysis using five concentrations of manganese ranging from 0.1 to 1.0 mg/L. The method showed a linear relationship between analyte concentration and peak area of manganese. The coefficient of determination (r²) for the line was 0.9997. Figure 2 shows the overlay of chromatograms of the working (calibration) standards, and Table 2 shows the concentrations of the working standards and the calibration result. Note that a 20 µL injection of the 0.1 mg/L standard produced a peak of significant size and good peak shape, whereas the nonsuppressed method in Reference 2 produced a small tailing peak for a 1 mg/L standard (though only a 10 µL injection). This highlights the expected sensitivity benefit of using suppressed rather than nonsuppressed conductivity detection.

Columns: Dionex IonPac CS12A Guard, 4 × 50 mm
Dionex IonPac CG12A Analytical, 4 × 250 mm
Eluent Source: Dionex EGC III MSA Cartridge with Dionex CR-CTC Column
Eluent: 20 mM MSA
Flow Rate: 1.0 mL/min
Inj. Volume: 20 µL
Temperature: 35 °C
Detection: Suppressed Conductivity, Dionex CSRS 300 Suppressor, 4 mm, Recycle mode, Current 60 mA
Sample: Standard Mixture

Peaks: 1. Lithium 1.0 mg/L
2. Sodium 1.0
3. Ammonium 1.0
4. Potassium 1.0
5. Magnesium 1.0
6. Manganese 1.0
7. Calcium 1.0

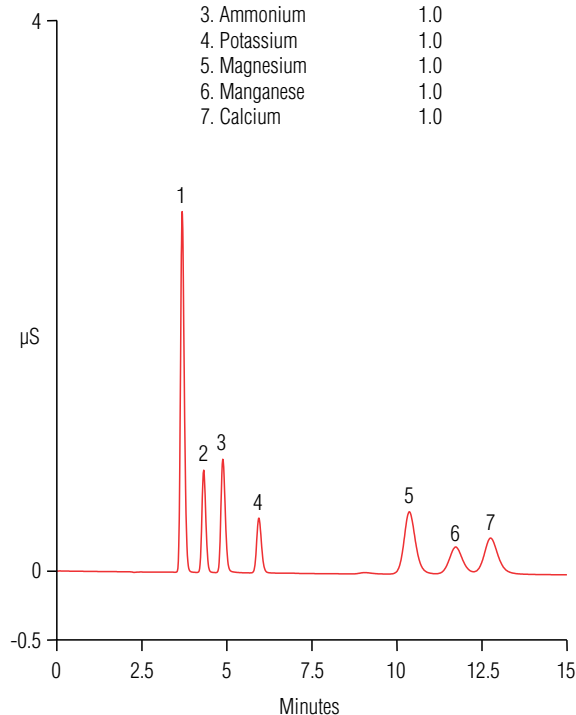


Figure 1. Chromatogram of a standard containing six common cations and manganese.

Columns: Dionex IonPac CS12A Guard, 4 × 50 mm
Dionex IonPac CG12A Analytical, 4 × 250 mm
Eluent Source: Dionex EGC III MSA Cartridge with Dionex CR-CTC Column
Eluent: 20 mM MSA
Flow Rate: 1.0 mL/min
Inj. Volume: 20 µL
Temperature: 35 °C
Detection: Suppressed Conductivity, Dionex CSRS 300 Suppressor, 4 mm, Recycle mode, Current 60 mA
Sample: Calibration Standard

Peak: 1. Manganese 0.1, 0.2, 0.4, 0.8, and 1.0 mg/L

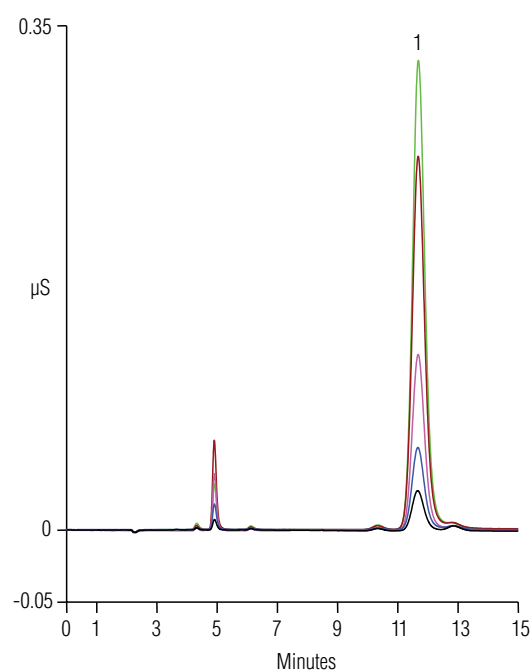


Figure 2. Overlay of chromatograms of the calibration standards.

Sample Analysis

An electrolyte sample was simulated as described in the Sample Preparation section and diluted 1 to 50 with DI water. Five sample injections were made and, as expected, no manganese was found in the simulated sample. A sample was then prepared to simulate manganese cathode dissolution in the electrolyte. This simulated sample had a manganese concentration of 0.1 mg/L after dilution. Five injections of the diluted spiked simulated sample were made to quantify manganese. The measured concentrations were then compared to the prepared concentration. This analysis yielded a manganese recovery of 103% with an RSD of 0.15% (Table 3).

Figure 3 shows the overlay of chromatograms of the simulated and spiked simulated samples. Note that the magnesium and calcium peaks—eluting before and after manganese, respectively—do not interfere with the quantification of manganese. Overall, the results indicate that this is an accurate and reproducible method for determining manganese in Li/LiMn₂O₄ battery electrolyte.

Conclusion

This study demonstrates an accurate and reproducible IC method that uses suppressed conductivity detection to determine manganese in the simulated electrolyte of a Li/LiMn₂O₄ battery. The method uses an RFIC system and requires only 15 min per analysis with a simple isocratic separation using an MSA eluent. The eluent is produced by an eluent generator to preclude the labor and potential error associated with eluent preparation.

References

1. Thermo Scientific Application Note 258: Determination of Tetrafluoroborate, Perchlorate, and Hexafluorophosphate in a Simulated Electrolyte Sample from Lithium Ion Battery Production. Sunnyvale, CA, 2010. [Online] www.dionex.com/en-us/webdocs/88116-AN258-IC-Lithium-Battery-AN70399_E.pdf (accessed Apr. 5, 2013).
2. Doh, C.; Lee, J.; Lee, D.; Jin, B.; Moon, S. The Quantitative Analysis of the Dissolved Manganese in the Electrolyte of Li/LiMn₂O₄ Cell Using by Ion Chromatography. Bull. Korean Chem. Soc. 2009, 30 (10), 2429–2432.

Columns: Dionex IonPac CS12A Guard, 4 × 50 mm
Dionex IonPac CG12A Analytical, 4 × 250 mm
Eluent Source: Dionex EGC III MSA Cartridge with Dionex CR-CTC Column
Eluent: 20 mM MSA
Flow Rate: 1.0 mL/min
Inj. Volume: 20 µL
Temperature: 35 °C
Detection: Suppressed Conductivity, Dionex CSRS 300 Suppressor, 4 mm, Recycle mode, Current 60 mA
Samples: Sample
Spiked Sample

Peak: 1. Manganese 0.1033 mg/L

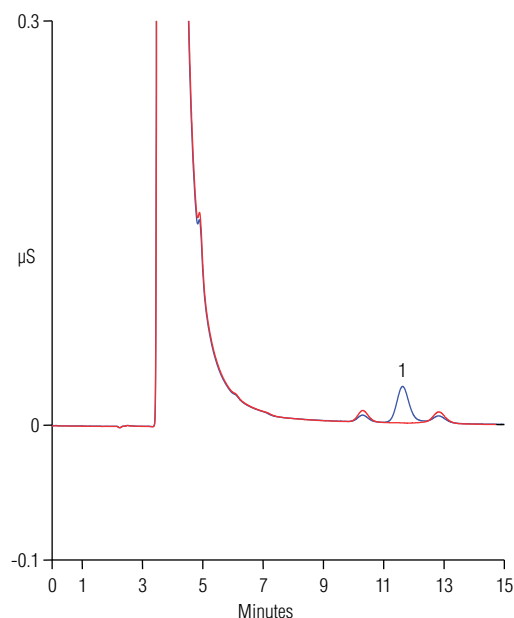


Figure 3. Overlay of chromatograms of unspiked and spiked samples.

Injection No.	Amount in Sample (mg/L)	Amount in Spiked Sample, Spiked Conc 0.1 mg/L (mg/L)
1	ND	0.1030
2	ND	0.1034
3	ND	0.1033
4	ND	0.1034
5	ND	0.1033
Average	ND	0.1033
RSD (%)	—	0.15
Recovery (%)	—	103

Table 3. Sample and spiked sample results.

Find out more at thermofisher.com/dionex

ThermoFisher
SCIENTIFIC

Simultaneous Determination of Impurities and Major Elements in Lithium-ion Battery Cathodes using the Thermo Scientific iCAP 6000 Series Radial ICP-OES

Authors

Marine Beauvir, ICP Application Specialist, Thermo Fisher Scientific, Cambridge, UK

Key Words

ICP-OES, Li-ion battery, cathode, elemental composition, impurities, QA/QC

Goal

Quality in material is often related to control of both major component and impurity levels. In this work, the Thermo Scientific iCAP 6000 Series ICP-OES was successfully used for the elemental composition analysis of lithium-ion (Li-ion) battery cathodes enabling concurrent determination of the concentrations of the material main constituents and trace elements.

Introduction

Li-ion Batteries, a Growing Market

Our energy dependence on fossil fuels, the implications for the economy, plus an increasing concern over greenhouse gas emissions and climate change have been driving the need for renewable energy and, in turn, efficient energy storage. Whether used in large-scale photovoltaic systems or to improve electric vehicle performances, advanced battery technologies are being developed. Li-ion batteries are in this sense relatively recent and a growing market. They are commonly used as rechargeable batteries in electronic devices such as mobile phones and computers, but they also have widely replaced nickel metal-hydride (NMH) batteries in hand-held tools. Li-ion batteries have high specific energy, cycle life and no memory effect. They are therefore considered as a suitable choice in demanding industries such as electric vehicle manufacturing. However, research and development on this technology is still very active, and the composition and structure of Li-based batteries in constant evolution.



Li-ion Cathodes

Compared to other types of batteries such as NMH, the composition of Li-ion batteries can vary significantly, depending mainly on the cathode composition, for example LiCoO_2 , LiMn_2O_4 , LiFePO_4 , $\text{LiNi}_{0.8}\text{Co}_{0.15}\text{Al}_{0.05}\text{O}_2$, etc. Lithium cobalt oxide (LCO) has historically been the material of choice for Li-ion cathodes and still represents a large part of the Li-ion battery market. However, LCO based batteries are known to have limitations and this combined to economic and environmental considerations means alternatives are already available and used commercially, or are being developed. Their composition varies from incorporating or replacing cobalt with other elements like manganese, nickel, aluminium to doping-coating the surface of the cathode. Structures of material are explored mainly to enhance cathode performances in terms of capacity, cycle life and lifetime.

During manufacturing process, the composition of each type of cathode itself is critical to obtain reproducible performances. Changes in raw materials or process conditions could affect the composition of the cathode, consequently affecting the quality of the battery. In particular, the presence and concentration of impurities is a key factor to cycle life, storage capacity and even safety of the Li-ion battery. Therefore, accurate determination of



the concentrations of both main elements and impurities in the cathode material is an important step in battery manufacturing. Whereas the main elements will be present at percentage level in the cathode material, specifications of impurities are generally around the ppm (mg/kg) level. Inductively Coupled Plasma Optical Emission Spectroscopy (ICP-OES) offers a perfect solution for elemental analysis. The usual approach taken by analysts is, after sample digestion, to determine the impurities in the prepared solution and perform a further dilution to capture the major elements of the cathode.

In this note, the wide dynamic range of the Thermo Scientific iCAP 6000 Series ICP-OES is fully utilised as a method was developed allowing simultaneous determination of main elements and impurities in one analysis. Direct advantages of this approach include less sample preparation, faster analysis turnaround time and therefore lower running costs.

Instrumentation

A Thermo Scientific iCAP 6500 ICP-OES with dedicated radial plasma view and standard sample introduction system was used for this work. This instrument configuration was chosen for its high matrix tolerance and reduced matrix interferences. A Thermo Scientific iCAP 6300 ICP-OES with dedicated radial plasma view is equally suited to this application and the parameters used apply to both model configurations.

Instrument Parameter	
Sample Pump Tubing	Orange/White Tygon
Pump Rate	50 rpm
Nebulizer Gas Flow	0.55 L/min
Auxiliary Gas Flow	0.5 L/min
Coolant Gas Flow	12 L/min
RF Power	1150 W
Radial Viewing Height	12 mm
Nebulizer	Glass Concentric
Spray Chamber	Cyclonic
Centre Tube	1.5 mm
Torch	EMT
Data Acquisition Mode	Speed
High/Low Integration Time	5/15 s
Replicates	3

Table 1. The instrument parameters used for analysis

Sample and Standard Preparation

An accurate mass of cathode material, approximately 0.5 g, was digested in a closed vessel at 160 °C for 1 hour using a mixture of analytical grade nitric and hydrochloric acids (50:50) and the final solution made up to 100 mL. The resultant acid concentration (2% v/v) was matched in all subsequent prepared standards and solutions.

The cathode specifications provided with the sample were the basis of the standard preparation assuming a 200 fold dilution. The concentrations of the multi-element standards used for analysis are listed in Table 2. They were prepared from certified standards, 1000 or 10,000 mg/L single element solutions. A standard check solution (QC) was similarly prepared at the concentrations indicated in Table 2. A 2000 mg/L manganese solution was also used for method development. A synthetic solution was prepared containing manganese, lithium and aluminium at respective concentrations of 2000 mg/L, 150 mg/L and 50 mg/L to mimic the sample composition. This solution was used in the method validation process for spike recoveries. Note that solutions containing high concentrations of manganese could be obtained after dissolution of a manganese salt, providing high purity of this salt. Yttrium was used as an internal standard at a concentration of 10 mg/L.

Element	Blank	Standard 1	Standard 2	QC
Mn	0	1500	3000	750
Li	0	150	300	75
Al	0	50	100	25
Na	0	20	40	10
S	0	20	40	10
Ca	0	2	4	1
K	0	2	4	1
Si	0	2	4	1
Cu	0	0.5	1	0.3
Fe	0	0.5	1	0.3
Mg	0	0.5	1	0.3
Ni	0	0.5	1	0.3
Zn	0	0.5	1	0.3

Table 2. Standard concentrations in mg/L

Method Development

For each element, several wavelengths were selected based on relative intensity, higher for impurities and lower for major components. The instrument was calibrated and the 2000 mg/L manganese solution analyzed. The sub-array plots were then examined by wavelength, assessing spectral interferences, selecting appropriate wavelengths and optimising background positions. High resolution of the optical system and full spectrum coverage of the Charge Injection Device (CID) detector makes the

Thermo Scientific iCAP 6000 Series ICP-OES the instrument of choice for this type of applications. From the line rich library, finding suitable analytical wavelengths (i.e. avoiding spectral interferences related to manganese for the impurities and finding lower sensitivity wavelengths enabling the determination of major elements) was a relatively trouble free step.

When the sample matrix was first analyzed, however, two of the wavelengths originally selected showed interferences from elements that were not suspected. As shown in Figure 1, the sub-array of Ni 341.476 nm indicated the presence of zirconium in the sample and inspection of S 182.624 nm showed the presence of boron. In this work, the concentrations of both elements were only estimated. Although S 182.624 nm could still be used for analysis and the boron interference negated by removing the right background point (as shown in Figure 1), Ni 341.476 nm was not fit for purpose without the inclusion of zirconium to the existing method. A simplified alternative was then taken and a more sensitive line was used for the determination of nickel (Ni 231.604 nm) with the addition of an Inter-Element Correction (IEC) to correct for the manganese contribution to the signal measured for nickel at this wavelength. An IEC was also applied to S 180.731 nm to correct for the manganese contribution observed. A comparison of the results with S 182.624 nm can be found in the discussion below for information. Both sub-arrays for Ni 231.604 nm and S 180.731 nm are shown in Figure 2. The manganese solution at 2000 mg/L was used for the calculation of the IEC factors. These factors are calculated easily and efficiently using the Thermo Scientific iTEVA Software tool.



Figure 1. Ni 341.476 nm and S 182.624 nm sub-arrays obtained for the sample and 2000 mg/L Mn solution

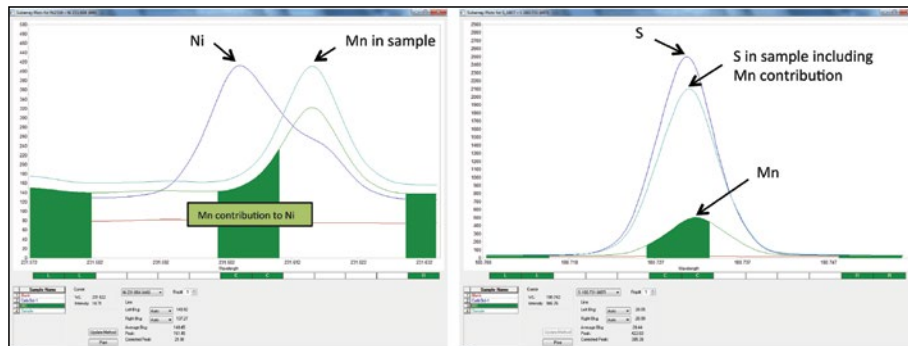


Figure 2. Ni 231.604 nm and S 180.731 nm sub-arrays obtained for the sample and 2000 mg/L Mn solution (used for IEC)

The final wavelengths selected in the method can be seen in Table 3.

Element	Wavelength
Mn	191.510 nm
Li	323.263 nm
Al	396.152 nm
Na	589.592 nm
S	180.731 nm*
Ca	393.366 nm
K	766.490 nm
Si	212.412 nm
Cu	224.700 nm
Fe	239.562 nm
Mg	279.553 nm
Ni	231.604 nm*
Zn	206.200 nm

*with IEC applied

Table 3. Elements of interest and selected wavelengths

Analysis and Results

Calibration was performed using the set of standards described above. A linear fit was used for all elements and coefficient of correlations were better than 0.9995 for all wavelengths. The QC standard was run immediately after calibration (QC initial) and at regular intervals within the analysis. Short term stability was demonstrated over a 3 hour period as shown in Figure 3.

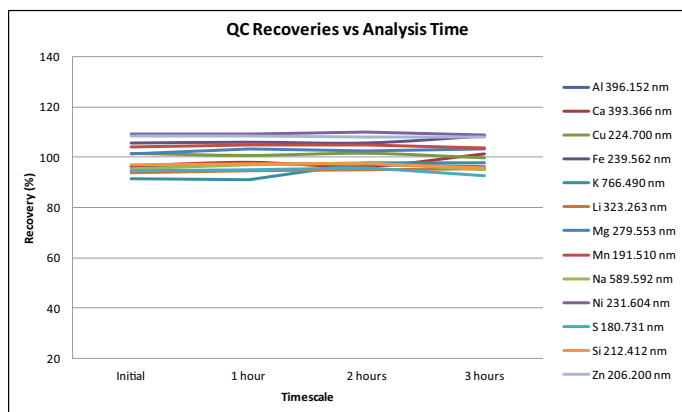


Figure 3. QC recoveries obtained over 3 hours

Method detection limits (MDL) are given in Table 4 for the impurities and are expressed as mg/kg in the original undiluted sample. Values were calculated using the average concentration and 3 times the standard deviation obtained from 10 replicates of a 2000 mg/L manganese solution with correction factor applied (approximated to 200).

Element	MDL (mg/kg)
Ca 393.366 nm	5
Cu 224.700 nm	1
Fe 239.562 nm	5
K 766.490 nm	10
Mg 279.553 nm	2
Na 589.592 nm	20
Ni 231.604 nm	5
S 180.731 nm	50
Si 212.412 nm	10
Zn 206.200 nm	2

Table 4. Method detection limits (mg/kg)

Results obtained for the cathode material are shown in Table 5. They are averages calculated from repeat analyses performed on 3 different days. The relative standard deviation on these combined measurements is also tabulated and was found to be below 5%. Concentrations obtained for sulphur from both wavelengths, S 182.624 nm (slight boron contribution) and S 180.731 nm (tabulated, IEC – manganese), were in good agreement with 2846 mg/kg and 2773 mg/kg respectively, although as expected, the concentration obtained from S 182.624 nm was positively biased. With no correction of the manganese contribution to S 180.731 nm, the apparent sulphur concentration in solution would have been 16.7 mg/L, of which 2.8 mg/L are really attributed to manganese. In sample term, this is equivalent to 3337 mg/kg “total” against 2773 mg/kg actual sulphur concentration. This observation demonstrates the advantages and capabilities of using the IEC approach inherent to the Thermo Scientific iTEVA Software suite to correct for spectral interferences. Boron and zirconium concentrations were estimated to be 400 mg/kg and 140 mg/kg respectively. As shown in Table 5, all major elements (manganese, lithium and aluminium) fell within specifications. All impurities were also below the specification limits required in this sample type.

	Measured Concentration	RSD (%)	Spec.
Major Element (% w/w)			
Al	1.4	1.8	1.1 – 1.5
Li	4.2	2.9	3.9 – 4.5
Mn	56	2.7	54 – 59
Impurity (mg/kg)			
Ca	171	1.0	<200
Cu	<1	-	<20
Fe	24	2.5	<70
K	388	3.5	<500
Mg	21	4.1	<100
Na	2340	2.5	<3000
Ni	<5	-	<100
S	2773	3.0	<5000
Si	45	2.2	<400
Zn	<2	-	<20

Table 5. Sample results obtained

These limits can be set within the Thermo Scientific iTEVA Software using the Corrected Limit Check (CLC) feature. As seen in Figure 4, a CLC check type was created and the sample specifications entered. When applied to an unknown sample, results outside the set limits will be flagged as the sample is analyzed. This is a useful QA/QC tool as out of specification samples are rapidly and easily noticed, and actions can be taken accordingly.

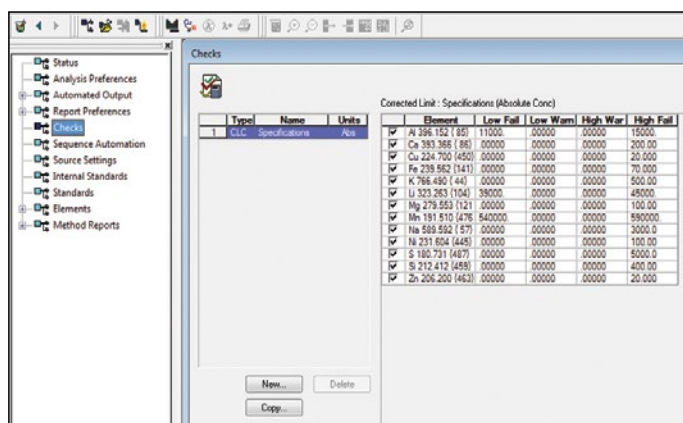


Figure 4. Corrected Limit Check feature

Finally, series of analyte spikes were performed on the prepared sample of the cathode material and synthetic solution. The sample was spiked with all impurities at approximately half the measured concentrations or 5 times the MDL for elements below the detection limit. Copper for example was spiked at 0.025 mg/L in solution which is equivalent to 5 mg/kg when expressed in sample term. As shown in Figure 5, good recoveries were obtained for calcium, copper, iron, magnesium, sodium, nickel and sulphur with a bias less than 10% of the expected value. Acceptable results were also obtained for potassium, silicon and zinc with concentrations within 15% of the expected value.

The synthetic solution with concentrations of manganese, lithium and aluminium similar to the cathode material studied was also spiked with the impurity elements. One set of spikes were performed at 5 times the MDL (i) and another set at half the measured concentrations in the original supplied cathode material sample (ii). As shown in Figure 5, good recoveries were obtained for all elements and at all levels of spiking. In addition, the major elements manganese, lithium and aluminium showed excellent recoveries in the synthetic sample at 102%, 97% and 99% respectively.

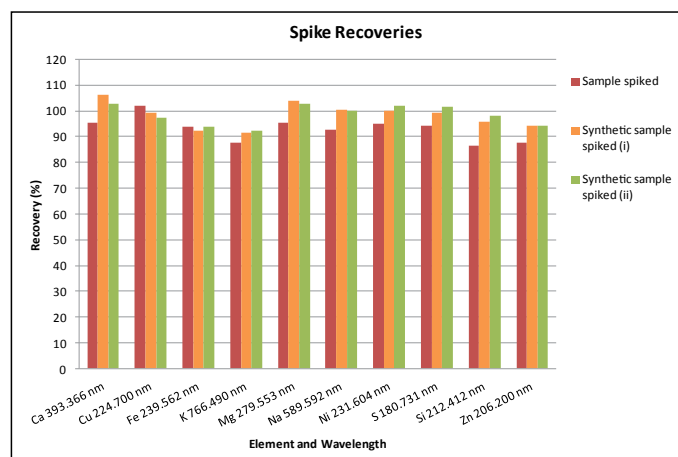


Figure 5. Spike recoveries of impurities in the cathode material and synthetic samples

Conclusion

A rapid, precise and accurate method for the simultaneous determination of major elements and impurities in a manganese based Li-ion battery cathode was developed successfully using a Thermo Scientific iCAP 6000 Series ICP-OES with dedicated radial plasma viewing. This work demonstrates the capability of the instrument to measure elements with concentrations in solution ranging from < 0.005 mg/L to nearly 3000 mg/L (i.e. 6 orders of magnitude) in a single analytical run. The combination of powerful optical design, CID detector technology and iTEVA Software features including the IEC correction approach allows the analyst to overcome the challenges of spectroscopic interferences easily and effectively in complex sample matrices. The instrument's unrivalled ease of use, with particular regards to the sample introduction system design and customized software tools helps users in their day to day analyses, making the iCAP 6000 Series ICP-OES the ideal robust instrument for QA/QC laboratories.

Orbitrap GC-MS Technology Provides New Insight into Lithium Ion Battery Degradation

“We can see many more compounds that we hadn’t seen before—including intermediates from the start of the reaction—which helps us establish reaction mechanisms.”

—Dr. Sascha Nowak, Head of the Analytics and Environment Division, MEET Battery Research Center, University of Münster

Advancing lithium-ion battery technology

From consumer electronics to electric vehicles, the growing demand for better-performing, safer, and less costly batteries has led researchers to focus on improving several aspects of lithium ion battery technology. Münster Electrochemical Energy Technology (MEET), the battery research center at Münster University, aims to address electrolyte aging, a major factor affecting lithium ion battery life. Using the Thermo Scientific™ Q Exactive™ GC Orbitrap™ GC-MS/MS system, MEET’s Analytics and Environment division gains a broader and deeper understanding of their samples that in turn provides new insight into the complex reaction mechanisms involved in electrolyte aging. Ultimately these insights will enable the research team to identify additives to curtail, or even halt, electrolyte aging.



© WWU/MEET

Electrolyte aging

Of the basic components of a lithium-ion battery, the electrolyte provides a conductive medium for lithium ions to move between electrodes. It consists of conducting solids, which are highly fluorinated, and various solvents. Lithium hexafluorophosphate (LiPF_6)-based electrolytes with mixtures of aprotic organic carbonate solvents are commonly used. As the electrolyte degrades, several decomposition complex products are formed, such as fluorophosphates and organofluorophosphates. Using a variety of analytical approaches, researchers at MEET's Analytics and Environment division identify and quantify these compounds as they are generated during aging.

Research challenges

There are significant challenges associated with this research. To begin, the degradation mechanisms, and the resulting degradation products, are often unknown and not described in published literature. Thus there are no reference materials available, and research published thus far has used low-resolution gas chromatography—mass spectrometry techniques (GC-MS)^{1,2}, nuclear magnetic resonance (NMR)³, and other techniques to identify compounds. Often these approaches do not provide sufficient structural information or sensitivity to detect and identify all compounds of interest. Moreover, some of the analytes are very small, low-molecular-weight molecules that, if fragmented, would be below the detection range of standard triple quadrupole GC-MS systems.

Another challenge is the complexity of the sample matrices studied, which are rich in highly fluorinated compounds and concentrated solvents. Matrix effects can lead to interferences, reduce instrument sensitivity, and increase instrument maintenance requirements.

“We have solvents that are highly concentrated, and the Q Exactive instrument is robust enough to handle these very well; such that we can do trace analysis.”

—Dr. Sascha Nowak



© WWU/MEET

“Because we’ve seen so many more compounds, the Q Exactive GC reduces the time it takes us to establish complete reaction mechanisms. And though in the future we will spend more time identifying all of these compounds; because we get additional fragmentation information from the Q Exactive, we will be able to do it much faster.”

—Dr. Sascha Nowak

Q Exactive GC Orbitrap GC-MS/MS solution

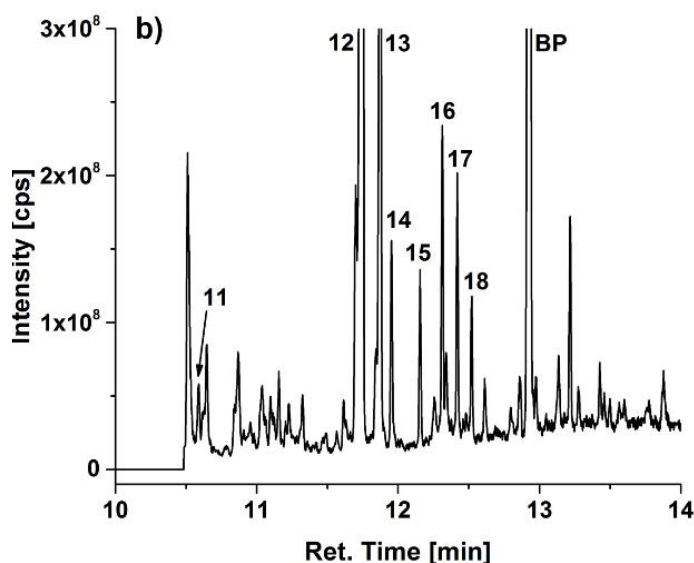
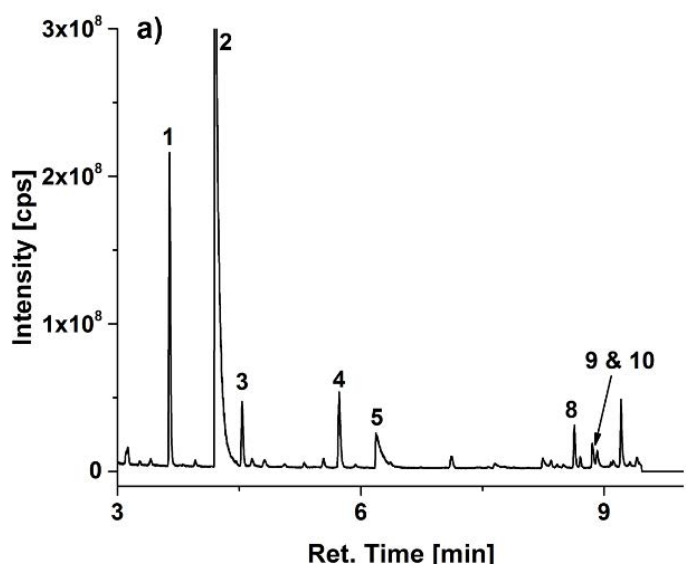
Using the Q Exactive GC Orbitrap GC-MS/MS system, MEET is now able to obtain lower detection limits and richer information in the form of accurate mass fragment ions and molecular ions produced by chemical ionization (CI). Compared to other approaches, this additional information enables MEET to detect and identify many more electrolyte degradation products. This in turn has enabled MEET to determine previously unknown, or confirm suspected, reaction mechanisms.⁴

High-capacity component detection with low limits of detection and matrix tolerance

Using other GC-MS technology, MEET typically detected about eight or nine decomposition products. When the same samples were analyzed with the Q Exactive GC Orbitrap GC-MS/MS system, MEET detected over forty compounds, a remarkable increase. MEET also found never-before-detected non-fluorinated hydrogen, carbon and oxygen-based compounds that improve their understanding of previously unknown mechanisms of solvent decomposition.

The new compounds, many of which were previously unknown early intermediates, were detected due to the sensitivity and selectivity of the Orbitrap GC-MS/MS instrument. Compared to other GC-MS approaches, the Q Exactive GC Orbitrap GC-MS/MS system improved detection limits from low mg/L to low ng/L levels, even in complex lithium-ion battery matrices.

Though the samples are rich in highly fluorinated compounds and concentrated solvents, the Q Exactive GC Orbitrap system provided exceptional robustness for trace-level analysis under these conditions. Continuous operation over the duration of research projects is commonly achieved.



Q Exactive GC Orbitrap GC-MS/MS system chromatograms of electrolyte extracted from an 18650 cell cycled at 20 °C diluted 1:10 in DCM with focus on the retention time from 3 to 10 min (a) and 10 to 14 min (b).



Conclusion

The Q Exactive GC Orbitrap system brings together the power of high-resolution GC and high-resolution accurate-mass (HRAM) Orbitrap MS to provide more comprehensive characterization of samples in discovery analysis. With the Q Exactive GC-MS/MS system, MEET accesses the exact mass information of more compounds, at significantly lower levels. The result is a broader and deeper understanding of the complex reaction mechanisms involved in electrolyte aging.

About Sascha Nowak

Sascha Nowak studied chemistry at the University of Münster, and obtained his Ph.D. in Analytical Chemistry. In 2009, Dr. Nowak joined the working group of Prof. Winter at the MEET Battery Research Center at Münster University as a postdoctoral researcher where he established the Analytical Department. From 2010–2012, he headed the competence areas Analytics and Recycling, and since 2012, has headed MEET's Analytics and Environment division, which mainly focuses on electrolyte aging, transition metal migration, and surface investigations, recycling, second life, and toxicological investigations.

About Münster Electrochemical Energy Technology (MEET)

Münster Electrochemical Energy Technology (MEET) is the battery research center at Münster University. It comprises an international team of about 150 scientists who work on the research and development of innovative electrochemical energy storage devices with high energy density, longer durability, and maximum safety. The aim is to improve batteries for use in electric cars and stationary energy storage systems at the lowest possible cost. MEET strives to further enhance the competitiveness of its partners in battery research—in particular on lithium-ion technology—both regionally and nationally.

The Analytics and Environment division is one of the three divisions at MEET. An important area of research for this division is electrolyte aging, which includes examination of electrolytes and migration of active material into the electrolyte, formation and properties of potentially toxic substances, and re-deposition of the migrated active material on the anode surfaces. The division also deals with the evaluation and development of recycling and second-life procedures to allow recovery and reuse of individual battery components or complete batteries.

References

1. Mönnighoff, X.; Murmann, P.; Weber, W.; Winter, M.; and Nowak, S. Post-Mortem Investigations of Fluorinated Flame Retardants for Lithium Ion Battery Electrolytes by Gas Chromatography with Chemical Ionization. *Electrochimica Acta*. 2017. 246: 1042–1051.
2. Mönnighoff, X.; Friesen, A.; Konersmann, B.; Horsthemke, F.; Grütze, M.; Winter, M.; Nowak, S. Supercritical Carbon Dioxide Extraction of Electrolyte from Spent Lithium Ion Batteries and its Characterization by Gas Chromatography with Chemical Ionization. *Journal of Power Sources*. 2017. 352, 56–63.
3. Wiemers-Meyer, S.; Winter, M.; and Nowak, S. Phys. Mechanistic insights into lithium ion battery electrolyte degradation—a quantitative NMR study. *Phys. Chem. Chem. Phys.* 2016.18, 26595–26601.
4. Horsthemke, F.; Friesen, A.; Mönnighoff, X.; Stenzel, Y.P.; Grütze, M.; Andersson, J.; Winter, M.; Nowak, S.; 2017. Fast Screening Method to Characterize Lithium Ion Battery Electrolytes by Means of Solid Phase Microextraction–Gas Chromatography–Mass Spectrometry. *RSC Advances*. 2017. 7: 46989–46998.



© WWU/MEET

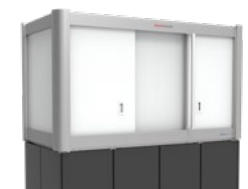
Find out more at thermofisher.com/OrbitrapGCMS

© 2019 Thermo Fisher Scientific Inc. All rights reserved. All trademarks are the property of Thermo Fisher Scientific and its subsidiaries. This information is presented as an example of the capabilities of Thermo Fisher Scientific products. It is not intended to encourage use of these products in any manners that might infringe the intellectual property rights of others. Specifications, terms and pricing are subject to change. Not all products are available in all countries. Please consult your local sales representatives for details. **CS10612-EN 0418M**

ThermoFisher
SCIENTIFIC

Battery Analysis Solutions from Thermo Fisher Scientific.

The preferred supplier for all your chemical, elemental and structural analysis needs in battery research, development and failure analysis.



microCT



TEM



FTIR



ICP-MS



Desktop SEM



XPS



GC



GC-MS



FESEM



XRD



NMR



Ion Chromatography



FIB-SEM



Raman



HPLC



LC-MS



Rheology



Twin-Screw Extrusion



Torque Rheometer



XRF

Find out more about Thermo Fisher Scientific capabilities for batteries at [**thermofisher.com/energy**](https://thermofisher.com/energy)

If you'd like to speak to an application specialist please visit [**thermofisher.com/specinquiry**](https://thermofisher.com/specinquiry)

ThermoFisher
S C I E N T I F I C